Radiation Effects on Photonic Imagers—A Historical Perspective

James C. Pickel, *Fellow, IEEE,* Arne H. Kalma, *Member, IEEE,* Gordon R. Hopkinson, *Member, IEEE,* and Cheryl J. Marshall, *Member, IEEE*

***Abstract*—Photonic imagers are being increasingly used in space systems, where they are exposed to the space radiation environment. Unique properties of these devices require special considerations for radiation effects. This paper summarizes the evolution of radiation effects understanding in infrared detector technology, charge coupled devices, and active pixel sensors. The paper provides a discussion of key radiation effects developments and a view of the future of the technologies from a radiation effects perspective.**

***Index Terms*—Active pixel sensor (APS), charge-coupled device (CCD), displacement damage, IR detectors, photonic imagers, total dose.**

I. Introduction

PHOTONIC IMAGERS operating in wavelength ranges from visible to infrared are being increasingly used in space-based systems, and exposure to the radiation environments in space poses a challenge to their functionality. Photonic imagers are subject to all the familiar radiation effects on room temperature microelectronics such as transients, total-ionizing-dose (TID) damage, displacement damage, as well as some additional concerns. The additional concerns are due to the low signal and noise levels, cryogenic operating temperature in the case of infrared detectors, and the unique physics of the devices.

The radiation effects community has been addressing photonics radiation effects issues in parallel with their technology development over the last three or four decades. Photonic imager technology has been developed for wavelength responses that range from ultraviolet (UV), through visible, to infrared (IR). Most radiation effects studies have been made on infrared detectors, and visible/near infrared technologies such as charge coupled devices (CCD), charge injection devices (CID), and more recently, active pixel sensors (APS). There have not been many radiation effects studies for UV imagers. This paper traces the evolution of radiation effects understanding in infrared detector technology, CCD detector technology and APS technology. Other important classes of photonics devices not covered in this paper include solar cells and fiber optics communication links. For each subject technology, the discussion is organized by a summary of the evolution of the technology, a discussion of key radiation effects developments in chronological order, and a view of the future of the technology from a radiation effects perspective.

Manuscript received March 11, 2003.

J. C. Pickel is with PR&T, Inc., Fallbrook, CA 92028 USA (e-mail: jim@pickel.net).

A. H. Kalma is with Science Applications International Corporation, Albuquerque, NM 87106 USA (e-mail: arne.kalma@saic.com).

G. R. Hopkinson is with SIRA Electro-Optics Ltd., U.K. (e-mail: gordon.hopkinson@siraeo.co.uk).

C. J. Marshall is with NASA Goddard Space Flight Center, Greenbelt, MD 20771 USA (e-mail: cmarshall2@aol.com).

Digital Object Identifier 10.1109/TNS.2003.813126

II. Infrared Detector Technology

Infrared detectors are a key element in many modern optical systems because of their thermal imaging capabilities. Their major advantage is the ability to detect a large fraction of the radiative emission from objects rather than relying on detecting light reflected off the objects, as is the case for visible detectors. For example, the peak emission from a 300 K blackbody is at $\sim$10 μm, and 99% of the emission from a 1000 K blackbody lies beyond 2.5 μm. Among the important applications of space-based infrared detectors are astronomy, earth surveillance from space, and missile detection and tracking.

Historically, the first materials used to fabricate infrared detectors were the lead salts, PbS with a cutoff wavelength between 2.5 μm and 4.0 μm and PbSe with a cutoff wavelength between 4.5 μm and 6.0 μm, depending on operating temperature. In the 1960s and 1970s, these began to be replaced as other materials such as InSb, doped germanium, doped silicon (which quickly replaced doped germanium), HgCdTe, PbSnTe (which was only investigated for a brief period until it was determined not to be any better than HgCdTe), and silicides began to be used and better detectors were developed. In the late 1980s and early 1990s, quantum well and superlattice detectors based on III–V materials were also developed. HgCdTe is currently the most widely used detector material, primarily because detectors with near-theoretical performance can be fabricated and the cutoff wavelength can be tuned between $\sim$1.5 μm and $\sim$20 μm by varying the Hg-to-Cd ratio. The cutoff wavelength of quantum well and superlattice detectors can also be tuned by varying the superlattice parameters. However, the quantum efficiency of these detectors has been low thus far, so they have not found the wide usage that HgCdTe detectors have, despite using a more common semiconductor material. While doped silicon and silicide detectors have the advantage of being based on silicon, doped silicon detectors (which can operate out to $>$25 μm) require very low operating temperature and the quantum efficiency of silicide detectors is very low, so use of these materials is also limited. The performance of InSb detectors, which have a cutoff wavelength of $\sim$6.0 μm, is quite competitive with that of similar HgCdTe detectors. However, the cutoff wavelength of InSb is fixed, so it cannot cover the range of applications that HgCdTe can.

TABLE I
WAVELENGTH REGIONS WHERE INFRARED DETECTORS OPERATE

Wavelength Region	Wavelengths (μm)	Detector Types
SWIR	1 – 3	**HgCdTe**, silicide, PbS
MWIR	3 – 5	**HgCdTe, InSb**, superlattice, silicide, PbSe
LWIR	8 – 14	**HgCdTe**, superlattice, doped germanium, PbSnTe
VLWIR	>14	**IBC silicon**, doped silicon, HgCdTe, superlattice, doped germanium

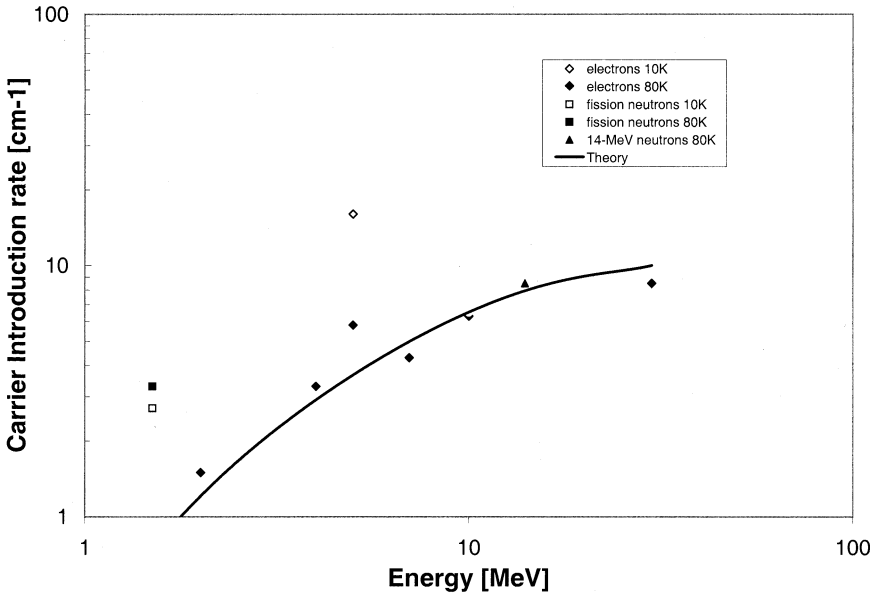

Fig. 1. Energy dependence of the carrier introduction rate in LWIR HgCdTe [7].

The first infrared detectors (PbS, PbSe, early HgCdTe, early doped Ge, and early doped Si) were photoconductive devices (i.e., a biased photoresistor whose resistance changes when illuminated). Although some photoconductive detectors are still used, these are being replaced by photovoltaic devices (i.e., zero- or reverse-biased diodes whose current increases when illuminated) that have the advantage of drawing much lower current for large array applications. Related to photovoltaic devices are the impurity band conduction (IBC) detectors (which are a high-low junction as opposed to a p-n junction) fabricated from doped silicon, and Schottky barrier detectors fabricated from silicides. There have also been some metal-insulator-semiconductor (MIS) detectors fabricated, especially from HgCdTe and InSb, but these have not received wide usage.

The infrared detection region is divided into several subregions. These regions and the detector types that operate in the regions are shown in Table I. The detectors shown in bold are the primary detectors in a region.

In part because of the pervasive nature of HgCdTe detectors, most of the reported radiation effects studies on infrared detectors have concerned HgCdTe. Therefore, we emphasize HgCdTe in the rest of this section and in general refer only briefly to studies in other materials.

A. Permanent Degradation

1) The Early Years: Single-Element Detectors and the Importance of Displacement-Damage-Induced Permanent Degradation: In a path very similar to that of silicon integrated circuit (IC) technology, the first infrared detectors were single element devices. They may have been passivated to stabilize the device properties, but they did not include insulators as an integral part of the active device. Therefore, displacement damage dominated the permanent degradation, and total-dose effects were not important. In the 1970s, there was a large number of studies performed to investigate displacement damage in HgCdTe material [1]–[18]. These publications discuss the effects of irradiation at 4.2 or 77 K on both the electrical and optical properties of LWIR material, and also contain detailed annealing information. Displacement effects in MWIR material have not been studied in detail, but one study [1] showed that MWIR material damages at a rate that is $\sim$1.5 times faster than does LWIR material.

The basic displacement damage effect of irradiating HgCdTe is the introduction of donors, probably Hg vacancies. The donor introduction rate in LWIR HgCdTe at 80 K is shown as a function of electron energy in Fig. 1 [7]. The theoretical curve shown in the figure is based on the non-ionizing energy loss (NIEL) of electrons and has been normalized to the experimental data. Also shown in the figure are the donor introduction rates for fission and 14-MeV neutrons and some data measured at 10 K. These radiation-induced donors are also Shockley–Read–Hall (SRH) centers that degrade the lifetime. Therefore, the donor introduction rates are also essentially the same rate at which recombination centers are introduced.

TABLE II
DEGRADATION THRESHOLDS IN VARIOUS DETECTORS

Detector Type	Radiation Environment	Irradiation Temperature (K)	Displacement Damage Threshold
LWIR HgCdTe	Fission Neutrons	78	~3x10^{14} n/cm^2
	14-MeV Neutrons	78	~1x10^{14} n/cm^2
	2-MeV Electrons	78	~6x10^{14} e/cm^2
	Co^{60} Gammas	78	~4x10^7 rd(HgCdTe)
Photoconductive InSb	14-MeV Neutrons	78	~5x10^{12} n/cm^2
Photovoltaic InSb (n/p)	14-MeV Neutrons	78	~3x10^{11} n/cm^2
Photoconductive PbS	Thermal Neutrons	300	~5x10^{15} n/cm^2
	14-MeV Neutrons	300	~2x10^{13} n/cm^2
	7.5-MeV Protons	300	~2x10^{12} n/cm^2
	12-MeV Protons	300	~7x10^{12} n/cm^2
	133-MeV Protons	300	~1x10^{13} n/cm^2
	450-MeV Protons	300	~2x10^{13} n/cm^2
Si:As	Fission Neutrons	10	~1x10^{11} n/cm^2

For an n-type photoconductive detector, the optical response (ΔV) can be shown to be

$$\Delta V = \frac{g \tau_m V}{n} \tag{1}$$

where g is the optical generation rate, τ_m is the majority-carrier lifetime, V is the bias, and n is the majority-carrier (electron) concentration [19]. The parameter found to be most sensitive to displacement damage is n [1]–[18]. Displacement-damage-induced donor introduction will increase the electron concentration, which in turn will degrade the optical response. For high performance, the initial donor concentration is made as low as possible, usually on the order of 1×10^{15} cm^{-3}. The addition of the same concentration of displacement-induced donors will degrade the optical response by a factor of two.

Photovoltaic detectors are diodes and are minority carrier devices. The best performance metric for photovoltaic detectors is the product of the resistance at zero bias times the detector area (R_0A). The best photovoltaic detectors are operated in the diffusion current regime, where the zero bias resistance is dominated by diffusion of minority carriers to the depletion region. Early detectors were all n-on-p devices with R_0A dominated by diffusion current from the p-type material. In this case, R_0A can be shown to be

$$R_0A = \frac{kTp\tau}{e^2 n_i^2 t} \tag{2}$$

where k is the Boltzmann constant, T is the temperature, p is the hole carrier concentration, τ is the minority carrier lifetime, e is the electron charge, n_i is the intrinsic carrier concentration, and t is the detector thickness [20].

Because the hole concentrations on the p side in these devices were relatively high, it would require the introduction of a significant concentration of displacement-induced donors to decrease this. Therefore, the parameter most impacted by displacement damage is the minority carrier lifetime. This lifetime will be degraded by the introduction of SRH centers. The initial SRH defect concentration in photovoltaic HgCdTe detectors is made as low as possible, often on the order of 1×10^{15} cm^{-3}. The introduction of the same concentration of SRH centers by displacement damage would degrade the R_oA by a factor of two.

Another damage mechanism that could impact the R_oA is lifetime degradation on the n side. The maximum minority carrier lifetime in n-type HgCdTe is set by the Auger lifetime, which varies inversely as the square of the electron carrier concentration [19]. For good performance, this electron carrier concentration is kept low, perhaps as low as 1×10^{15} cm^{-3}, so the Auger lifetime on the n side can be approximately as sensitive to displacement-damage-induced effects as the minority carrier lifetime on the p side.

The estimated degradation thresholds, defined as the fluence at which the responsivity degraded by a factor of two, for HgCdTe and other detector types are shown in Table II. In three studies [21]–[23], photovoltaic HgCdTe detector arrays were exposed up to a level of $\sim 2 \times 10^{13}$ n/cm^2 (fission neutrons), which is less than the estimated degradation threshold, without observing any displacement-induced degradation. By this exposure level, the accompanying total dose had begun to produce degradation, as will be explained in the next section.

One study of fast neutron (14- or 15-MeV) damage in InSb photoconductive and photovoltaic detectors has been reported [24]. The photoconductive detectors were p-type, and the hole removal rate was found to be 1.1 cm^{-1}. This resulted in a slight increase in the optical response of photoconductive detectors beginning at a fluence of $\sim 5 \times 10^{12}$ n/cm^2. The photovoltaic detectors were n-on-p devices whose leakage current was dominated by generation-recombination current from the more lightly doped n-type base region. The most radiation-sensitive parameter in these devices was the minority carrier lifetime in the n region. The impact of neutron irradiation on R_0A was not reported, but the optical response degradation threshold was reported to be 3×10^{11} n/cm^2. These degradation thresholds are shown in Table II. Modern photovoltaic (PV) InSb is based on p-on-n diodes. While some limited gamma and proton

damage data have been obtained on p-on-n InSb, damage thresholds have not been reported.

Electron- and fission-neutron-induced damage has been reported on p-type PbSnTe material [25], [26]. Irradiation with 30-MeV electrons at 78 K produced a hole carrier addition rate of 3.6 cm^{-1} in more lightly doped (4×10^{16} cm^{-3}) material, but a hole removal rate of 22 cm^{-1} in more heavily doped (8×10^{17} cm^{-3}) material. When more heavily doped (4×10^{17} cm^{-3}) material was irradiated at 9 K, the carrier removal rate was 9 cm^{-1}. The authors hypothesized that the reason for the difference was that both donors and acceptors were produced, but whether or not the donors were fully ionized depended on the location of the Fermi level and thus on the doping level in the material. Fission-neutron irradiation of a more heavily doped (4×10^{17} cm^{-3}) material at 78 K resulted in a carrier removal rate of 42 cm^{-1}. No irradiation studies of actual PbSnTe detectors have been reported. Nor is there any information available about the material parameters that would be used in detectors. Therefore, we cannot estimate the degradation thresholds for detectors.

Displacement damage produced by thermal neutrons [27], 14-MeV neutrons [28], [29], or protons [27], [30] in PbS photoconductive detectors has been reported. PbS detectors are usually operated with internal gain (G), which is the ratio of the material lifetime (τ) to the sweepout time (t_s) in the device. The optical responsivity (R) in such a detector can be written as

$$R = \frac{\eta G e \lambda}{h c} \tag{3}$$

where η is the quantum efficiency, λ is the wavelength, h is Planck's constant, and c is the speed of light. The sweepout time can be written as

$$t_s = \frac{1}{\mu E} \tag{4}$$

where μ is the mobility and E is the field across the detector. Thus

$$G = \tau \mu E \tag{5}$$

and

$$R = \frac{\eta \tau \mu E e \lambda}{hc}. \tag{6}$$

The only parameters in this equation that can be affected by displacement damage are the mobility and the lifetime, with the lifetime being by far the more sensitive. However, the reports did not provide enough information to determine any material parameters, so we can only summarize the degradation threshold. The fluence at which the responsivity degraded by a factor of two for each particle type investigated is shown in Table II. Although not always stated, it is likely that all of these PbS tests were performed at room temperature.

There has also been one report of fission-neutron damage in arsenic-doped silicon material at 10 K [31]. In doped-silicon detectors, the optical response is proportional to the majority carrier (electron) lifetime, which is inversely proportional to the concentration of recombination centers. In n-type doped-silicon detectors operated at 10 K, all of the electrons are frozen out on the donor sites, but some donor sites are empty due to the presence of compensating acceptor sites. It is these empty donor sites that serve as the recombination centers for the optically excited electrons. The concentration of compensating acceptor sites is kept as low as possible for long lifetime and high performance. In the tested material, the acceptor concentration was $\sim 5 \times 10^{13}$ cm^{-3}, but can be as low as $\sim 2 \times 10^{12}$ cm^{-3} in high quality detectors. As additional compensating acceptors are introduced by irradiation, the lifetime, and thus the optical response, degrades. The measured acceptor introduction rate was 16 cm^{-1} in both float-zone (low oxygen concentration) and pulled-crystal (high oxygen concentration) samples. This neutron-induced response degradation remained approximately the same for annealing temperatures, as high as 673 K. This resulted in a factor of two response degradation after exposure to $\sim 3 \times 10^{13}$ n/cm^2 in the tested material, but the degradation threshold could be as low as $\sim 1 \times 10^{11}$ n/cm^2 in detectors fabricated from higher quality material. This degradation threshold is shown in Table II.

2) The Intermediate Years: The Advent of Multielement Arrays and the Importance of Total-Dose-Induced Permanent Degradation: In the late 1970s and early-to-mid 1980s, development shifted to multielement detector arrays. These required surface passivation between the individual detector elements. In HgCdTe arrays, the most common architecture was n-on-p photovoltaic detectors passivated with a deposited layer of ZnS. ZnS is very effective at trapping charge, so total-dose-induced permanent degradation became much more important than displacement effects. As a result, many studies were reported that investigated the mechanisms of total-dose-induced effects in arrays and how one might harden against them [21], [32]–[41]. Most of the early hardening approaches involved investigation of alternate passivation insulators such as anodic sulfide [43], [44] or deposited SiO_2 [33], [45]. Occasionally, unpassivated devices were also investigated [37]. While some quantitative differences were observed, both MWIR and LWIR devices exhibited similar behavior.

Studies of the C–V characteristics of MIS capacitors demonstrated that both electrons and holes could be trapped in ZnS, with the net charge depending on the sign of the bias applied across the ZnS [32]–[35], [42]–[45]. The total-dose-induced trapped charge in the ZnS causes a shift in the surface potential in the HgCdTe. The magnitude of the applied bias and the surface treatment of the HgCdTe control the amount of charge trapped and thus the size of the potential shift, as shown in Fig. 2 [33]. Even at relatively high bias, the net trapped charge is only a few percent of the total charge produced in the ZnS by the irradiation.

At zero bias, the sign of the net trapped charge can be positive or negative, depending on the surface treatment of the HgCdTe and perhaps other factors (e.g., stray fields). Therefore, the ionization-induced trapped charge in the ZnS can either cause accumulation or depletion (and eventually inversion, leading to increased crosstalk due to the presence of a conducting path between detector elements) of the HgCdTe surface between the diodes. In either case, this causes an increase in the surface leakage current and degraded array performance, as shown in Fig. 3 [21]. ZnS is so effective at trapping charge that HgCdTe

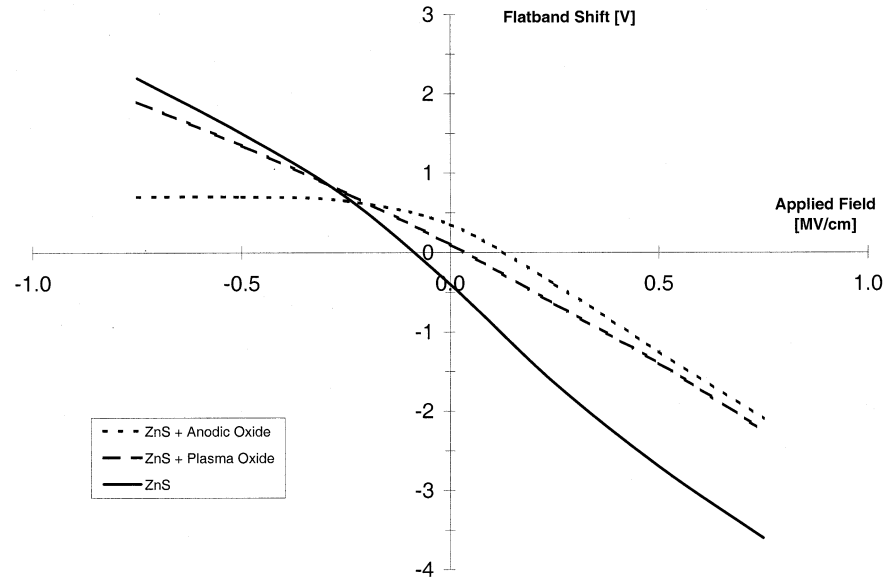

Fig. 2. Total-dose-induced flatband shift in HgCdTe MIS capacitors with ZnS insulator and different surface treatments. Total dose $= 6.8 \times 10^3$ rd(ZnS), $T = 77$ K [33].

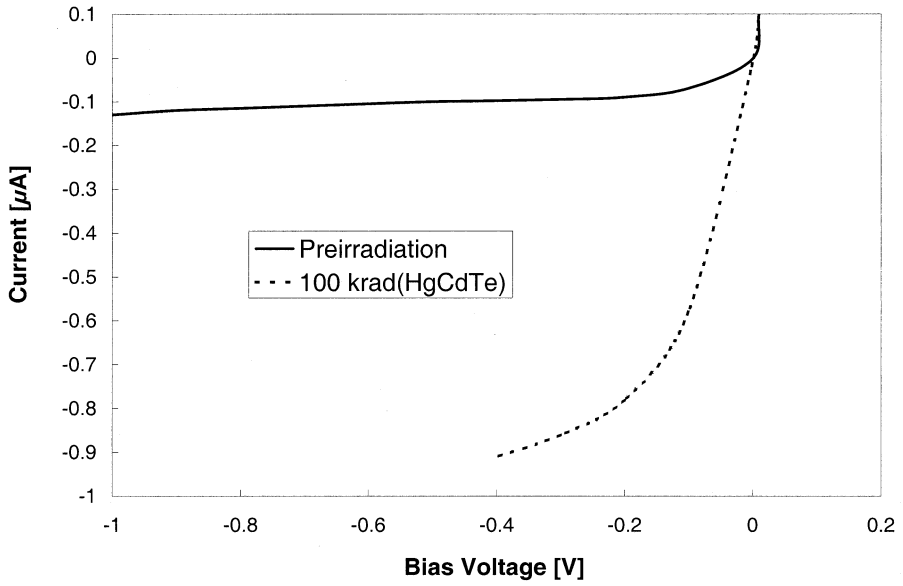

Fig. 3. Total-dose-induced increase in leakage current in ZnS-passivated HgCdTe diodes. Total dose = 1e5 rd(HgCdTe), $T = 125$ K [21].

arrays passivated with it exhibited degradation at low exposures that ranged from $\sim 3 \times 10^3$ rd(ZnS) to $\sim 5 \times 10^4$ rd(ZnS). In general, detectors with higher initial quality (e.g., higher R_0A) exhibited less total-dose vulnerability. However, these high-quality total-dose-hard detectors could not be reproduced consistently, nor could they be produced uniformly across full arrays. Thus, while there was an existence proof that high-quality rad-hard detectors could be produced, by the late 1980s, it was becoming clear that ZnS passivation was not the solution.

The finding that detectors with high initial quality generally were also more total-dose tolerant led to the eventually accepted hypothesis that the mechanism that caused high total-dose vulnerability was related to the cause of poor detector performance. Therefore, it was thought that solving the problem of poor detector performance would likely result in total-dose hardness as well. In addition, it was clear that the state of the interface between the HgCdTe and the passivation was key to device performance and hardness and that developing a high quality interface that could be fabricated reproducibly was the most important issue.

While use of alternate passivation materials (e.g., anodic sulfide, deposited SiO_2, or silicon nitride) sometimes decreased the total-dose vulnerability of HgCdTe arrays, the improvement was not enough to be called a solution. In particular, high performance and hardness could not be obtained consistently. Unpassivated devices were found to be hard to $\sim 3 \times 10^6$ rd(HgCdTe), as shown in Fig. 4 [37]. However, passivation for providing device stability is even more important for HgCdTe devices than it is for silicon devices, so elimination of the passivation was

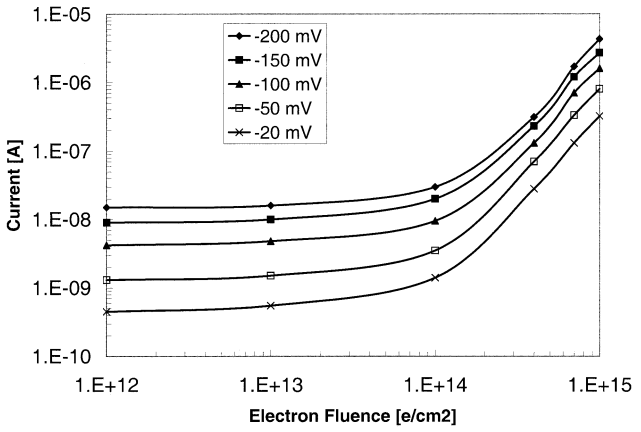

Fig. 4. Total-dose-induced increase in leakage current in unpassivated HgCdTe diodes. $T = 77$ K [37].

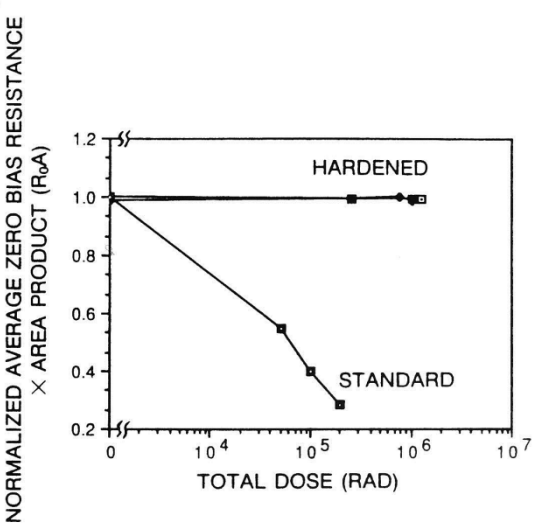

Fig. 5. Improved total-dose hardness in CdTe-passivated HgCdTe arrays. $T = 80$ K [22].

not an acceptable option. All of the ionization-induced trapped charge was found to anneal out by 300 K. Thus, periodic heating of HgCdTe arrays could effectively remove all the radiation damage. However, this was not a solution that could be used in all systems. The eventual solution was the development of CdTe passivation, to be discussed in the next section.

No total-dose tests of InSb detector arrays have been reported. However, there has been one report of MIS capacitor tests [46]. The insulator in these tests was silicon oxynitride, which probably contained little or no nitrogen. Whether or not this insulator is similar to what is used in InSb arrays is not known. The radiation response of this silicon oxynitride was very similar to that of thermally grown SiO_2 on silicon when irradiated at low temperature, which means that it was not very radiation tolerant. Exposure to 1×10^4 rd(SiO_2) produced flatband shifts of $\sim$0.1 V at 0 V applied bias and $\sim$0.5 V at 1e6 V/cm applied bias in 110-μm-thick insulators. For photovoltaic detector arrays with a substrate doping of $\sim 3 \times 10^{15}$ cm^{-3}, we can estimate that significant surface potential shifts would be produced by exposure to $\sim 5 \times 10^3$ rd(SiO_2).

There has been one reported total-dose test of PbSnTe arrays [21]. Measurable leakage current increase was observed in detectors on one array after exposure to $\sim 1 \times 10^5$ rd(PbSnTe), while no change was observed in detectors on a second array after exposure to 4×10^5 rd(PbSnTe). All of the damage in the one array annealed out by 300 K.

3) The Recent Years: The Use of CdTe Passivation and the Development of Mega-Rad-Hard Arrays: In the late 1980s and early 1990s, most manufacturers of HgCdTe arrays successfully developed CdTe passivation, which is much more compatible with HgCdTe than was ZnS or any of the other passivations used earlier. The driving force behind the development of CdTe passivation was improved detector and array performance, especially for LWIR devices. The CdTe approach proved very successful, as high performance detectors and uniform arrays (with fewer bad elements) were produced. At the same time as the switch to CdTe passivation occurred, most manufacturers also shifted from n-on-p architectures to p-on-n architectures. While use of the p-on-n architecture did lead to revolutionary changes in device performance (especially when combined with CdTe passivation), its impact of total-dose hardness was at most evolutionary. Higher total-dose hardness was primarily the result of using CdTe passivation.

A desirable side effect of using CdTe passivation, but not one that was the primary thrust of the development, was that the arrays also were much harder to total-dose exposure [22], [23], [47]–[52]. It was found that CdTe-passivated HgCdTe detectors would survive exposure to >1 Mrd(HgCdTe), as shown in Fig. 5 [22]. This meant that the total-dose hardness of a hybrid array was no longer controlled by the response of the detector array, but was controlled by the hardness of the MOS readout.

Since the detector array and readout integrated circuit are hybridized through indium bump bonds and the detectors must be operated at cryogenic temperatures, the readouts are also operated at cryogenic temperature. Total dose effects are more severe in cryogenic CMOS than at room temperature because of enhanced charge trapping the oxides. Hybrid arrays with unhardened readouts tend to fail after exposure to a few tens of krd(SiO_2). It is possible to obtain hardened readouts that will survive up to one Mrd(SiO_2) at cryogenic temperature but, as is the case for room-temperature electronics, the cost of rad-hard readouts is high and the number of process lines that are willing to fabricate them is diminishing. Fortunately, the trend toward use of higher density CMOS processes is also favorable to total dose hardness since oxides are thinner and inversion thresholds tend to be higher for scaled processes. Use of hardness-by-design practices and submicron processes has allowed radiation-tolerant readouts to be fabricated in commercial foundries that are acceptable for many uses in the natural space radiation environment.

B. Ionization-Induced Transient Response

1) Single Event Pulses and Noise: While permanent degradation is an important aspect of the radiation response of infrared detectors, ionization-induced transients are often more important issues in actual applications. In order to detect optical photons, infrared detectors must be very sensitive ionization detectors. They must be able to detect low energy IR photons and this requires a low noise floor. As a result, they

are also extremely effective detectors of ionization, often being able to sense individual particles. This is akin to single event transients caused by heavy ions in standard integrated circuits, except that the sensitivity of infrared detectors is so great that they can often detect single electrons. In fact, infrared detectors are often designed using the same principles used to design nuclear detectors. Some of the earliest investigations of the radiation response of infrared detectors were driven by the need to understand their response to fluxes of ionizing particles. The two main applications that drive concerns for transients are strategic systems that are concerned about the effects of gamma and electron flux and astronomy systems that are concerned about the effects of cosmic rays.

a) Gamma-Induced Pulses: Most of the reported studies of the response of infrared detectors to gamma-flux exposure have been for HgCdTe detectors [21]–[23], [36], [53]–[55] with one report [21] also including PbSnTe detector response. When detectors are exposed to a gamma flux, a distribution of pulses is produced. A typical distribution is shown in Fig. 6 [21]. Most of the pulses are not the result of direct interaction of the gammas with the detector. Rather, the gammas interact with the surrounding material and produce secondary electrons through Compton scattering and photoelectric effect, which in turn interact with the detector. The primary reason a distribution of pulse amplitudes is produced is because of the varying path lengths that the electrons traverse through the detector volume. A secondary reason is differences in the energy loss rate of different energy secondary electrons.

In order to calculate the gamma-induced pulse amplitude distribution in a detector with high fidelity, one needs to perform a radiation transport calculation through the surrounding material. Unfortunately, these are not simple analytic calculations that are easy to perform. Further, transport codes often truncate their calculations at a finite electron energy, which ignores electrons that can be significant in producing the pulse amplitude distribution in detectors.

Fortunately, there is a semi-empirical method of making estimates of the pulse amplitude distribution that is analytic and relatively easy to use [56]. The average chord length ($\overline{C}$) in a rectangular volume is

$$\overline{C} = \frac{2}{1/x + 1/y + 1/t} \tag{7}$$

where x, y, and t are the dimensions of the volume. Some of the Compton electrons (usually between 5% and 10%) stop or start within the detector. To allow for these, a term is added empirically to the equation, and one finds the average electron path length ($\overline{L_e}$) in the detector to be

$$\overline{L_e} = \frac{2}{1/x + 1/y + 1/t + 2/\overline{L_c}} \tag{8}$$

where $\overline{L_c}$ is the average path length of the average-energy Compton electron in the detector material.

The average pulse amplitude $\overline{n}$ in carrier pairs is then

$$\overline{n} = \frac{\overline{E}\,\overline{L_e}}{\overline{L_c}\varepsilon_p} \tag{9}$$

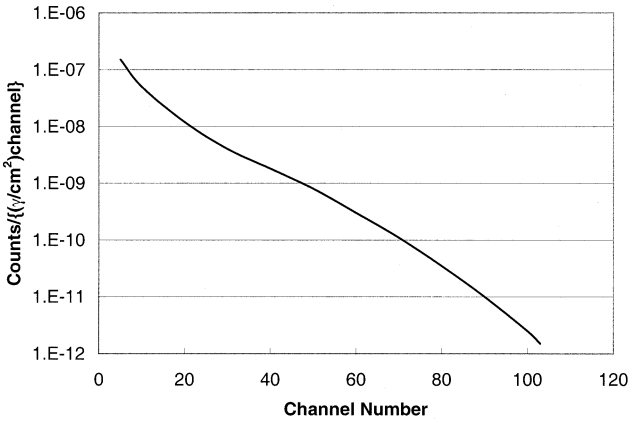

Fig. 6. Gamma-flux-induced pulse amplitude distribution in HgCdTe detectors. $T = 77$ K [21].

where $\overline{E}$ is the average energy of the Compton electrons produced by the gammas and ε_p is the energy required to create a carrier pair in the material.

The internal event rate (R_i) produced by the gammas interacting directly with the detector can be shown to be [56]

$$R_i = \mu V \varphi_\gamma \tag{10}$$

where μ is the linear absorption coefficient of the gammas in the material, V is the detector volume, and φ_γ is the gamma flux. The external event rate (R_e) produced by the Compton electrons from the surrounding material interacting with the detector is [56]

$$R_e = \frac{\mu\left[(xy + xt + yt)\,\overline{L_c}\right]\phi_\gamma}{2}. \tag{11}$$

The total event rate (R) is just the sum of the internal and external event rates.

Although Pickel and Petroff [56] also developed an expression for the pulse amplitude distribution, it is not of simple analytic form and requires a computer code for solution. Most users of this semi-empirical approach simply rely on the observation that the pulse amplitude distribution is approximately exponential and determine the predicted distribution from the calculated average event amplitude and total event rate. This tends to underpredict the number of pulses at low amplitude and overpredict the number at high amplitude. It is generally believed that exponential approximation gives results that are within an order of magnitude at all amplitudes (except very large ones where an exponential distribution remains finite but the real distribution drops to zero) and that are within a factor of two at most amplitudes.

The gamma-induced pulses in a detector result in increased noise. The measured gamma-induced rms noise in HgCdTe and PbSnTe detectors is shown in Fig. 7 [21].

The equation to calculate the noise squared (N_γ^2) produced by events with a distribution in amplitudes is

$$N_\gamma^2 = 2Rt_{\text{int}}\overline{n^2} \tag{12}$$

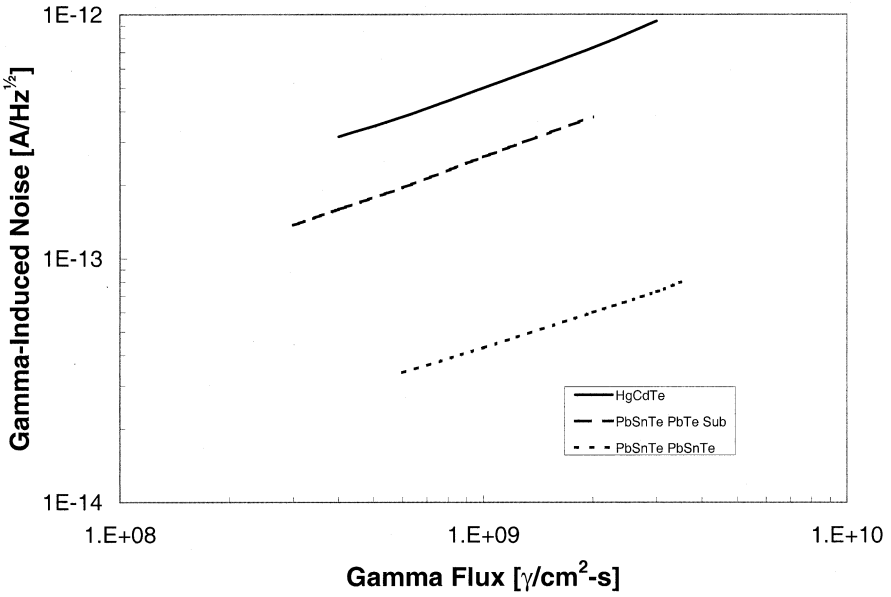

Fig. 7. Gamma-flux-induced noise in HgCdTe and PbSnTe detectors. $T = 77$ K [21].

where $t_{\rm int}$ is the integration time and $\overline{n^2}$ is the second moment of the amplitude distribution of the events. For an exponential distribution of amplitudes

$$\overline{n^2} = 2\overline{n}^{\,2} \tag{13}$$

where $\overline{n}$ is the first moment of the distribution and is the same as the average pulse amplitude calculated from (9). Using (9)–(13), one finds that

$$N_\gamma = \left[\frac{2\overline{E}\,\overline{L_e}}{\overline{L_c}\varepsilon_p}\right]\left[\mu\left\{xyt+\left(\frac{xy+xt+yt}{2}\right)\overline{L_c}\right\}\varphi_\gamma t_{\rm int}\right]^{1/2}. \tag{14}$$

In a similar manner, one can show that the gamma-induced noise current (i_γ) produced by an exponential distribution of pulse amplitudes is

$$i_n = \left[\frac{2\overline{E}\,\overline{L_e}e}{\overline{L_c}\varepsilon_p}\right]\left[\mu\left\{xyt+\left(\frac{xy+xt+yt}{2}\right)\overline{L_c}\right\}\phi_\gamma \Delta f\right]^{1/2} \tag{15}$$

where Δf is the bandwidth of the measurement.

The prefactor $(\overline{n^2}/\overline{n}^{\,2})^{1/2}$ in this analysis—the prefactor is $2^{1/2}$ in this case of an exponential distribution such as was used to obtain (14) and (15)—has been defined by some [57] as the shot noise multiplier. It varies depending on the shape of the distribution but can be readily calculated if the shape is known analytically or from experimental data.

There have been some device-level approaches postulated for separating the optically induced charge from the ionization-induced charge in extrinsic silicon and superlattice detectors. These have sometimes been termed intrinsic event discrimination (IED). The underlying premise is that the two energy states for the ionization-induced charge are the valence and conduction bands in the material, while one of the states for the optically induced charge is a bound state (e.g., an impurity level in an extrinsic detector or a bound state in a superlattice). However, no IED device concept has been fully demonstrated, and there are significant questions about how well (or even whether) such a device will eliminate the ionization-induced response.

b) Cosmic Ray-Induced Pulses: Cosmic ray-induced transients present a significant challenge for IR detector arrays used in space-based astronomy. Read noise specifications on the order of ten electrons or less, concomitant with very long integration times of several hundred to thousands of seconds, are often required. With these performance requirements and operation in space, the radiation environment from galactic cosmic rays (GCR), trapped particles, and energetic solar particles can dominate the noise [121]. This effect can often be managed at the system level since imaging arrays normally have nondestructive readout capability. That is, the signal charge can be sampled multiple times on a pixel-by-pixel basis during the integration time without disturbing the integrated charge. This procedure enables signal processing algorithms to recognize and remove the charge-contaminated pixels that have suffered a particle transient.

2) Low-Dose-Rate Effects: Some extrinsic detectors, especially doped silicon and doped germanium, display another type of response when exposed to a flux of ionizing particles while operated at low temperature and low optical background. The optical response increases while the detector is exposed to the ionization flux and then decreases when the flux is removed. These effects can occur at low dose rates and the time constants involved can be quite long. An example for an arsenic-doped silicon detector is shown in Fig. 8 [58]. In this case, the time constants were tens of seconds. At even lower optical backgrounds, time constants on the order of hours or even days have been observed. The phenomenon was termed the "gamma response anomaly" when it was initially observed. The cause is the filling of empty sites at which optically excited carriers would recombine by the ionization-induced charge. For example, in arsenic-doped silicon, the ionization-induced electrons fill the compensated (and thus empty) arsenic donor sites. It is the empty recombination sites that control the lifetime of the optically excited

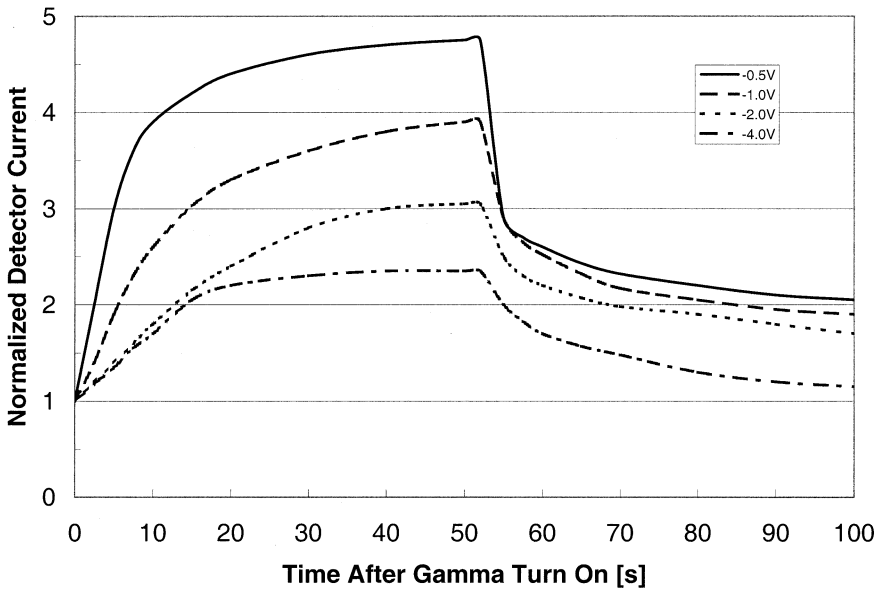

Fig. 8. Long equilibration times exhibited by extrinsic photoconductive detectors operated at low temperature and low optical background. Arsenic-doped silicon, operating temperature = 4.3 K, optical background = 8×10^{12} photons/cm^2-s, gamma flux = 10 rd(Si)/min. Gamma flux initiated at $t = 0$ and halted at $t = 52$ s [58].

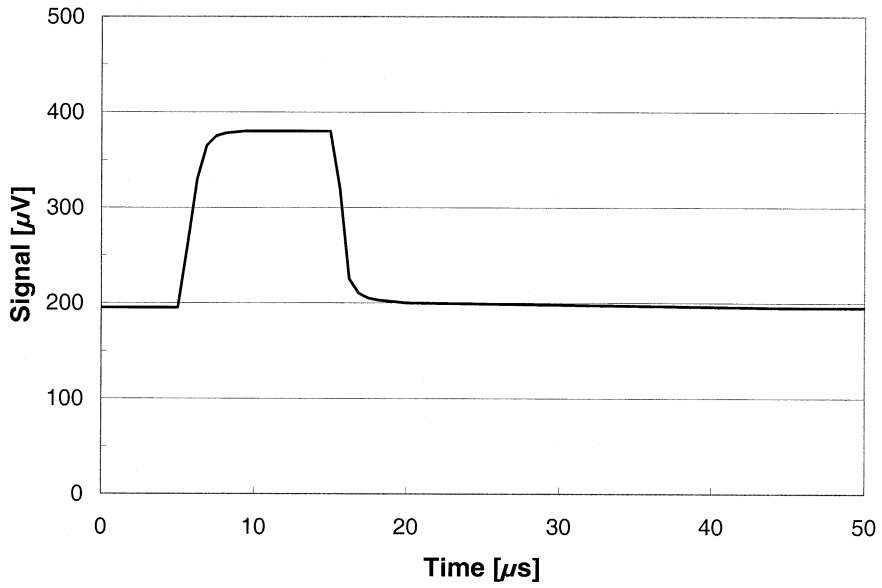

Fig. 9. IBC silicon detectors operated at low temperature and low optical background exhibit much shorter equilibration times. IBC arsenic doped silicon, operating temperature = 6 K, electron flux = 4e9 e/cm^2-s. Electron flux initiated at $t = 5$ μs and halted at $t = 15$ s [59].

electrons and thus the optical response in extrinsic detectors, so filling these sites increases the lifetime and causes an increased response. The time constants are long because there are few carriers available at low temperature and background, and it takes a long time for the device to reach a new equilibrium when a change is made. This is a process akin to dielectric relaxation. In fact, similar long-time-constant changes were subsequently observed when other changes (e.g., optical level, temperature) were made.

The long time constants and the pervasive nature of the gamma-response anomaly in extrinsic silicon detectors was a major driving force behind the development of IBC silicon detectors. The IBC devices are essentially a reverse biased high–low junction with a band of donor sites which can exchange charge with each other, instead of the donor sites being isolated and not able to interact with each other such as is the case in doped silicon detectors. As a result, it is easier to reestablish equilibrium in IBC detectors when changes are made, and the time constants are much faster (on the order of microseconds) [59], [60], as can be seen in Fig. 9 [59].

3) Prompt-Pulse-Induced Transients: When an infrared detector is exposed to a high-dose-rate ionization pulse (a prompt pulse), the individual events are no longer distinguishable, and a large current pulse is observed [21]–[23]. It is easy to calculate the magnitude of the charge produced (Q_ϕ) by the ionizing pulse if the detector volume is known. One starts with the dose

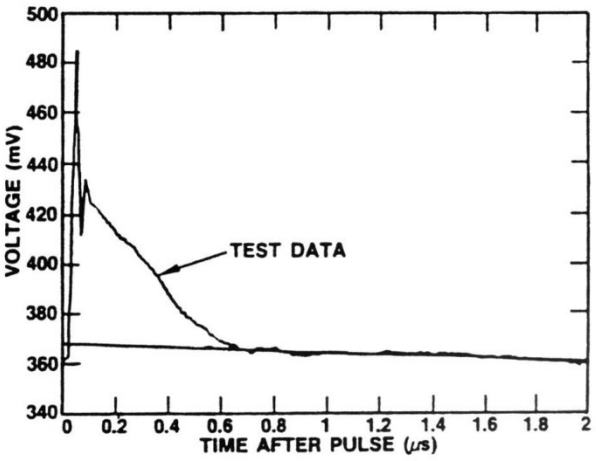

Fig. 10. Prompt pulse response of a HgCdTe detector. X-ray pulse of 2.5e9 rd(Si)/s, pulse width = 20 ns, $T = 80$ K [22].

rate and multiplies by the pulse width to get the dose deposited (ϕ) (or uses ϕ itself if this is what is known). One then uses the definition of dose (1 rd = 100 ergs/g), performs a units conversion to get this in units of eV/cm^3, divides by the energy required to create a carrier pair (ε_p), and multiplies by the electron charge and detector volume (V) to find

$$Q_\phi = \left[\frac{\phi \rho V}{\varepsilon_p}\right] \bullet 10^{-5} \tag{16}$$

where ρ is the density of the detector material. The temporal response of infrared detectors to a prompt pulse is generally controlled by circuit parameters and not the detector itself. The rise time of the response usually follows the ionization pulse, with the decay time determined by how fast the circuit can remove the ionization-generated carriers. An example of prompt pulse response is shown in Fig. 10 [22].

The magnitude of the prompt-pulse response is quite large in any infrared detector type, even for very low dose rate prompt pulses. As a result, the prompt pulse response of infrared detectors will almost always produce a response pulse that is large compared with the optical signal. Whether or not this large ionization-induced pulse upsets a system depends of other factors such as the recovery time and the sensitivity of subsequent electronics. However, most optical sensors are designed to ignore glitches, and prompt-pulse-induced glitches can be filtered out of the data stream as long as the recovery time is sufficiently fast.

III. Visible/Near Infrared Imager Technology

Visible and near-infrared imager technology has been developed in the form of CCDs, passive pixel arrays such as CIDs, and active pixel arrays such as APS. CCDs provide the lowest noise but consume the most power, are the most expensive, and suffer from radiation-induced charge transfer problems. CIDs avoid charge transfer problems with random readout and since they are CMOS compatible, they have low power consumption and are less expensive. However, they have larger noise than CCDs and are unacceptable for many low-noise applications. Recent developments with active amplification within the pixel has led to the active pixel sensor with all the advantages of the CID but much lower noise. APS technology is currently under development. Most of the radiation considerations for the APS imagers also apply to CID imagers, both being dominated by radiation effects in the CMOS circuitry. The following sections discuss evolution of radiation effects understanding for CCD and APS technologies.

A. CCD Imagers

CCDs were originally designed for use as memories, signal processing circuits, imagers, and readout circuits for infrared detectors. Some of these areas have now declined but use of CCDs as imaging detectors for the visible region remains widespread.

A CCD consists of an array of MOS capacitors. Fig. 11 shows the basic structure, typically built on a p-type epitaxial layer on the order of 10–20 μm thick. Potential wells are created by applying a voltage to one of the gate electrodes. The n-type buried channel ensures that the potential minimum is situated $\sim$1 μm into the silicon so that charge is kept away from the silicon–silicon dioxide interface. Charge is moved from one pixel to another by switching the applied voltage from one electrode phase to the next, first vertically, one row at a time, (in parallel) to the serial register where each row is moved one pixel at a time, to the readout amplifier. Three or four clock phases/pixel are commonly used for vertical transfers and two or three for serial (the former requires an implant to define the sense of direction).

Devices without a buried layer are known as surface channel and have the advantage of a higher charge handling capacity which is useful in IR detectors. However, MOS readout circuits are now used almost exclusively for this application and surface channel CCDs are rarely used today.

Since the charge transfer process is essentially lossless and the noise introduced by the readout amplifier is small (often just a few electrons rms), CCDs are almost perfect detectors for visible photons. This makes them especially vulnerable to displacement damage since even single atomic defects in the bulk of the lattice can cause observable dark current or trapping effects. In addition, buildup of ionization-induced charge in the gate dielectric and interface trap generation will (as in any MOS device) cause flatband voltage shifts that change the effect of the applied bias and clock voltages and generate thermal leakage (dark) current at the surface. As well as this permanent damage, transient effects will be produced by the charge deposited in the silicon by charged particles and X-ray or gamma ray photons.

Two recent books [61], [62] discuss the details of CCD operation and both have interesting sections on their early history and development. Radiation effects in CCDs have been discussed in [63] and [64]. Although the fundamental damage mechanisms and basic CCD architecture have not changed since the CCD was first described in 1970 by Boyle and Smith [65], there are several factors which have stimulated continued interest. A variety of device modifications and new operating techniques have been developed to enhance performance or to mitigate radiation effects and advances in silicon processing technology have led to large increases in device size (and number of pixels). It has always been difficult to predict the effect of radiation on image quality from device theoretical simulation alone because

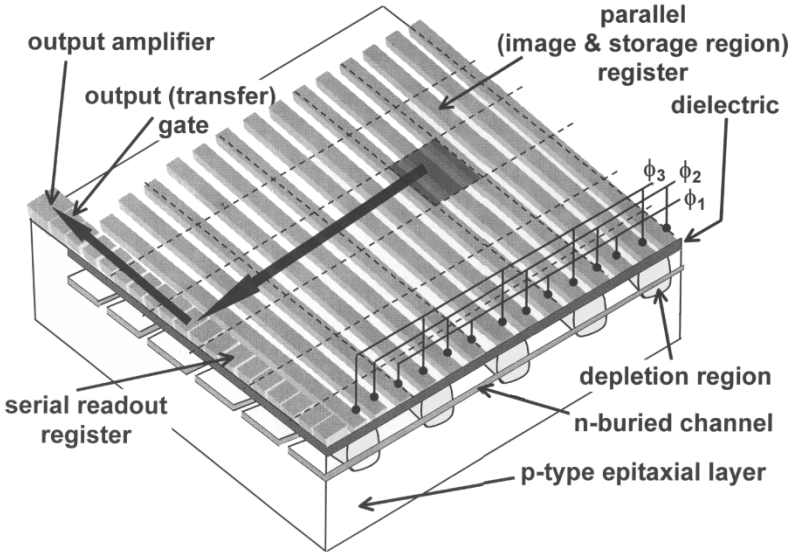

Fig. 11. Schematic diagram of an n-channel CCD.

of subtle dependencies on operating conditions (such as temperature and clocking rate). It usually requires an experimental effort to validate performance for each particular application. It should be borne in mind that CCDs are almost always commercial-off-the-shelf devices. Specifically hardened devices are sometimes manufactured but, even then, radiation performance is not often guaranteed by the manufacturer.

1) The Early Years (1970–1982): It was quickly realized that CCDs would be useful for military and space applications and that radiation effects needed study. This early work was reviewed by Killiany in 1978 [66]. The main emphasis was on neutron and gamma damage on the linear and small ($\sim$100 $\times$ 100 pixel) area device available at the time. The chief parameters of interest were flatband voltage shift, charge transfer efficiency (CTE), and increases in the average dark current level. The devices were not large enough, and "cosmetic" quality not good enough, for pixel-to-pixel differences in dark current to be a major issue.

In 1974, Mohsen and Tompsett [67] introduced the basic equations for charge transfer degradation when there are traps present in the buried channel. Three years later, Saks [68] discussed the traps created in a n-channel CCD by fast neutron irradiation and found trap energy levels at 0.14, 0.23, and 0.41 eV below the conduction band. He identified the A-Center (oxygen-vacancy complex) as responsible for the first of these, the divacancy for the second, and a mixture of divacancy and the E-Center (phosphorous vacancy complex) for the third. Today, the separation of the $\sim$0.4 eV level into the E-center and the divacancy is still not conclusive, though the recent interest in cooled CCDs for space astronomy has spurred a renewed interest in the defects responsible (see, for example, [69]–[71]). Recent work suggests that the E-Center is responsible for roughly 80% of the CTE degrading traps and that there is at least one other defect level at around 0.3 eV.

The relationship between displacement damage and bulk dark current was also being explored. In 1979, Srour *et al.* [72] gave an analytical model for dark current generation in depletion regions. The bulk defect responsible was not conclusively identified, but Srour *et al.* [73] recently gathered together the early data correlating damage for different radiation sources and silicon dopings, as well as data from subsequent CCD tests. They concluded that the divacancy is the dominant defect that generates bulk dark current and defined a universal damage constant. The value proposed was $(1.9 \pm 0.6) \times 10^5$ carriers/cm^3-s per MeV/g at 300 K and 1 week after irradiation (after a large fraction of any annealing has taken place).

The linear relationship between interface trap density and surface dark current was defined by Saks in 1982 [74]. In 1980, Saks *et al.* [75] recognized that by inverting the CCD surface so that it becomes accumulated with holes, the surface traps become filled and dark charge generation is suppressed. Soon afterwards multiphase pinned (MPP) CCDs were developed in which the whole (or almost the whole) surface could be inverted. This led to significant hardening to total ionizing dose (TID) as surface dark charge generation is no longer significant (as long as the surface remains inverted).

We have mentioned that flatband voltage shift is also caused by TID. It was recognized that normal CCD gate oxides were fairly radiation-soft and significant efforts were made to harden them (see, for example, [76] and [77]). Much of this work was for surface channel devices and low temperature operation and for structures, such as stepped oxide electrodes and charge injection gates, which are no longer relevant.

Another issue that received interest during the early years was the generation of transient events, particularly by high dose rates of gamma ray photons. In 1981, this work culminated in two papers [78], [79] which described the way that the noise generated by high dose rates of gamma radiation increases the random noise in an image. See [80] and the references therein for a recent discussion of transient effects.

2) The Intermediate Years: CCD Technology Matures (1983–1990): During the 1980s, the size and cosmetic quality of CCDs improved substantially and CCD instruments were designed for many applications, including space. For example

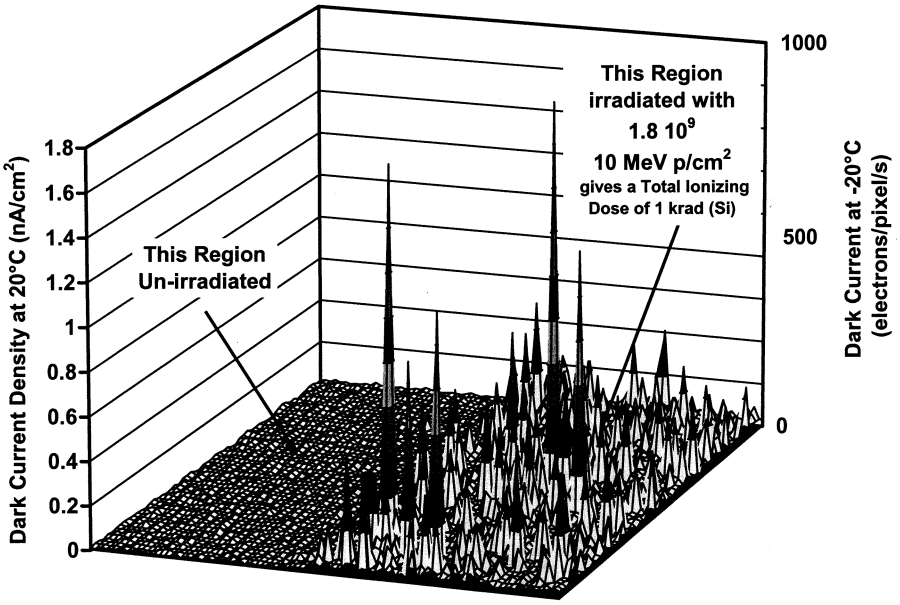

Fig. 12. Dark current spikes in a proton-irradiated CCD.

using CCDs in star trackers became common, at least for high accuracy applications and several focal planes were developed for space-based astronomy and planetary science (e.g., the 800 $\times$ 800 CCDs for the Hubble Space Telescope (HST) [81] and the Galileo mission [82]).

In the early-mid 1980s, several studies [83]–[86] looked at single neutron and proton effects. These are caused by both elastic collisions (Coulombic scattering and elastic nuclear scattering) and inelastic collisions (nuclear reactions). This work and the general need to look at effects in the new design of space-borne instruments led to the widespread realization that proton-induced dark current spikes were important for space applications. Fig. 12 shows dark current spikes due to protons. There was some work on CTE effects during this time, but the full consequences of displacement damage were not demonstrated until later. Dark current nonuniformity was particularly bad for virtual phase CCDs where the substitution of an implant for one of the electrode phases (to improve UV response) resulted in high electric fields within the depletion region.

Three papers [87]–[89] were presented at the 1989 IEEE Nuclear and Space Radiation Effects Conference, which gave evidence that dark current spikes can be caused not only by inelastic collisions (which deposit a large amount of energy and so create a large number of defects) but also by elastic collisions which happen to occur in high field regions of the depletion volume. In these cases, the dark current can be enhanced by several orders of magnitude due to field-enhanced emission. A characteristic of this phenomenon is that the dark current nonuniformity changes more slowly with temperature. In many cases, there is a clear correlation between the size of a dark current spike and the decrease in activation energy. At about the same time, Marshall *et al.* [90] produced a model for predicting dark current nonuniformity distributions in the absence of field enhanced emission. (See Robbins [91] for some later modifications to the model.)

As mentioned above, much of the early displacement damage work was with monoenergetic neutrons. During the 1980s, the concept of NIEL was developed by Burke and coworkers at NRL. This followed on from several earlier studies on the correlation of damage between different particles and energies (see, for example, [92]). The NIEL concept allows prediction of displacement damage dose (in megaelectronvolts/gram) which plays an equivalent role to total ionizing dose for ionization damage effects. The reader is encouraged to refer to [63] for a detailed discussion of NIEL damage scaling and its limitations. Values of NIEL for protons on silicon have been summarized by Dale *et al.* [93]. A recent update is given in [94]. There are some small differences between these results and earlier values, but these are comparable with the uncertainties involved (both in the calculations and in experimental data). For example, the ratio of the predicted NIEL for 10 and 60 MeV protons is 2.2 from [93] and 3.3 from [94].

3) The Recent Years: Radiation Effects Widely Studied (1991–Present): During the 1990s, many groups were involved in studying radiation effects in CCDs. Work for the Chandra [70], XMM-Newton [95], ASCA [96] and HST [97]–[99] programs showed that proton-induced CTE degradation can be very important, particularly at low signal levels. CTE degradation for higher temperature applications, such as star trackers, was also discussed [100]. Dale *et al.* [101] demonstrated the usefulness of the NIEL hypothesis for proton-induced CTE damage. CTE degradation has a strong dependence on background signal level, clocking rate (dwell time within a pixel), and temperature as well as on the signal size. Fig. 13 [100] shows typical results for a CCD with pixel size 22.5 $\times$ 22.5 μm (including channel stops). The dominant defect for CTI (CTI = 1-CTE) damage has an energy level of 0.44 eV [71] and at low temperatures can be kept permanently filled, thus significantly improving the charge transfer efficiency.

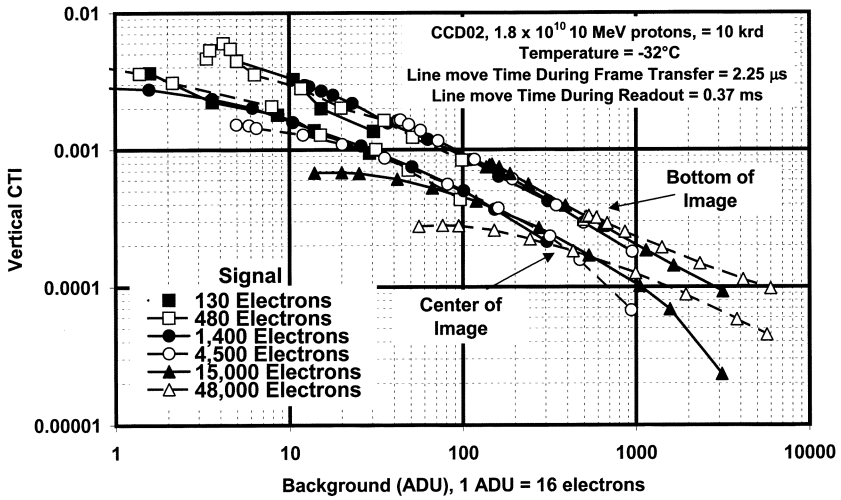

Fig. 13. Vertical CTI for an E2V CCD02 [100].

The data discussed above allows an approximate scaling of CTI values for different applications but the accuracy of those predictions is probably a factor of two at best. Hence, it is recommended to perform proton testing for the actual device operating conditions whenever possible. Even if the CTI is known, the effect on imaging performance still has to be calculated. Several authors [102], [103] have developed models for predicting CCD performance for particular operating conditions, but care is still needed to extrapolate results to other situations. Even for high signal applications, where CTI damage is reduced, CCDs are restricted to displacement damage doses below $\sim 5 \times 10^8$ MeV/g. Although a reduction in CTI damage can be achieved by heating the device, the temperature needs to be 100 °C or more and is not normally practical. Use of p-channel, rather than n-channel CCDs to eliminate the E-Center defects, has been studied [104]–[106] but requires specially designed CCDs.

Recently, it has been discovered that some pixels in postirradiated CCDs show a dark current that is not stable in time but switches between levels [107], [108]. This is called random telegraph signal (RTS) behavior. RTS behavior in CCD dark current has also been seen on-orbit [109]. Usually only a small fraction of pixels show large fluctuations, but many show low level changes and these have to be taken into account whenever dark signal nonuniformity is important for an application.

During the 1990s, several studies looked at ionization-induced effects. A typical flatband voltage shift for a commercial off-the-shelf (COTS) CCD is 0.1 V/krd(Si) [110] when biased and around one-half to one-third that value when unbiased during irradiation. This shift can affect the performance of the output amplifier for doses of 10 krd(Si) or more and will shift the clock voltage at which inversion (MPP operation) occurs toward more negative values.

It was mentioned above that inverted mode operation suppresses ionization damage-induced surface dark charge. Burke and Gajar [111] showed that continuous clocking (sometimes called dither clocking) can keep interface traps filled even in non-MPP CCDs. If surface dark charge is not suppressed, then it is often found that it is increased (by a factor ~ 2) under metallizations, such as used for the storage region light shield and for masking dark reference pixels. Fortunately, many space applications involve doses below 10 krd(Si) and TID is not an issue. A degree of hardening can be achieved by thinning the dielectric layer and also by balancing the electron and hole trapping in dual oxide/nitride dielectrics. However, there is often a reduction in manufacturing yield for such specialized devices.

Since COTS CCDs are not generally suitable for high total dose applications (>a few tens of kilorad) or for high proton fluences, other commercial devices such as hardened charge injection devices (CID) or active pixel sensors have to be used. CIDs avoid the charge transfer problem since the photo-charge is integrated in the pixel and read out through a CMOS multiplexer. However, CIDs are inherently noisier than CCDs.

B. APS Technology

In recent years, cost-effective radiation-tolerant active pixel sensor arrays have become an important alternative to charge coupled device arrays for some space applications without specialized requirements such as ultra-low noise performance. For APS imagers, each pixel has its own output amplifier and this improves the noise performance compared to CIDs. The pixels can be randomly accessed and nondestructive readout capability allows noise performance approaching CCDs. The inherent advantages of APS technology result from utilization of standard CMOS design and processing and include the possibility of highly integrated and functional, yet low power, imaging systems (i.e., "camera-on-a-chip" [112]). However, fixed pattern noise (both pixel-to-pixel due to variations in offset and column-to-column due to variations in readout circuitry) remains a challenge in the case of APS technology. For space applications, APS are advantageous in that pixels are directly addressed so there are no proton-induced charge transfer losses such as those experienced with CCD arrays. However, APS arrays are subject to increases in dark current, dark current nonuniformity, fixed pattern noise, and random telegraph noise as a result of proton exposure. There is also the potential for latch-up as a result of the on-chip signal processing circuitry.

To date there are a modest number of publications that treat the radiation response of APS technology. At the 1999 Radiation Effects in Components and Systems (RADECS) Conference, Cohen and David presented ^{60}Co and proton irradiation results on both photogate and photodiode based APS devices fabricated at the Austria Micro System (AMS) process line [113]. They showed that the dark current, dark current nonuniformity, and fixed pattern noise are key parameters that degrade under irradiation, with the largest performance loss in the photogate technology. In a second paper [114], the authors show that the radiation-induced loss in performance is dominated by ionizing damage effects which is to be expected from the soft CMOS technology employed in their work.

In a subsequent effort, photodiode APS devices fabricated using the 0.7 μm twin-well p-substrate process of Alcatel Microelectronics by IMEC, Belgium, have been well characterized. ^{60}Co results on the photodiodes, including those designed for increased radiation tolerance, have been reported [115] as well as ^{60}Co, proton and heavy-ion results on a 512×512 array [116]. Proton-induced dark current increases and hot pixel formation were similar to that observed for CCDs. The dark spikes were shown to result from electric field enhancement [116], [117] though the amplitudes were less than observed in a typical CCD. Random telegraph signal behavior was observed in the brightest pixels and in about 50% of all pixels by both Hopkinson [116] and Bogearts *et al.* [118]. Hopkinson found that the RTS fluctuations were a large fraction of the total signal in the APS devices, in contrast to the largest CCD fluctuation of $\sim$10% [116]. ^{60} Co testing showed large increases in dark current above about 6 krd(Si) but they annealed to a low level after a 100 °C bake [116]. It is interesting that the APS devices did show a decrease in responsivity after proton irradiation ($\sim$30% loss after 7.2×10^9 p/cm^2 at 10 MeV). The responsivity loss persisted for seven months but eventually annealed between 7.5–14 months after irradiation [116]. In contrast, responsivity changes have not been noted for CCD technology. No latch-up was observed in the APS device for 28 MeV/mg/cm^2 Ar ions up to a fluence of 2×10^6 ions/cm^2 in testing that was limited by beam constraints [116]. Although the analog-to-digital converter (ADC) latched as described in [116], Hopkinson noted that it was an old design that was slated for replacement.

Bogaerts *et al.* [117] have performed in-depth characterizations of the Ibis4 (standard) and STAR-250 (radiation hardened by design) CMOS photodiode APS from FillFactory. Although the STAR-250 device can tolerate a 10 Mrd(Si) exposure to ^{60}Co, it exhibits dark current increases, dark spike behavior, and RTS as reported for the unhardened devices [116]–[118]. It is worth noting that the rate of increase of the dark current was less than that observed for a typical CCD as a result of the much smaller pixel active column, even though the pre-irradiation dark current is significantly higher than obtained for CCD technology.

The radiation tolerance of APS can be improved via hardening-by-design at a commercial foundry [117], [119] or by fabrication at a rad-hard foundry such as BAE Systems. The radiation tolerance of the Photobit APS sensors up to total ionizing dose levels of 30 Mrd(Si) was reported in [117], as a result of hardening-by-design. The primary impact of the ^{60}Co gamma irradiation of the devices was a linear increase in the dark current with total ionizing dose at a rate of 1–2 pA/cm^2/krd(Si) at room temperature dependent on the pixel design. The thin gate oxide ($\sim$7.0 nm) contributed to the radiation hardness of all four of their pixel designs by assuring low threshold voltage shifts. The heavy-ion response of the Photobit APS imaging technology and the efficacy of hardening-by-design for transient ion effects was measured and modeled in 2002 [120], [121]. The transient ionization response was found to be very sensitive to photodetector design. Belredon *et al.* [122] have performed very detailed charge collection modeling on photogate and photodiode APS devices for the purpose of developing an on-orbit charged particle detector.

IV. Summary and Future Directions

A. IR Detectors

Radiation effect mechanisms in IR detectors continue to require attention as the technology evolves and applications become more demanding. Total-dose-induced degradation is an important damage mechanism in modern infrared detector arrays, particularly for strategic applications. HgCdTe technology has solved the total-dose problem in detectors by using CdTe passivation. The issue has not been addressed in most other detector technologies, so there may be technologies that are still vulnerable to total-dose exposure. In addition, all detector array technologies, including those where the detectors are total-dose hard, are subject to the total-dose vulnerability of the readout integrated circuit. While total-dose-tolerant MOS readouts exist, fabrication lines which can process such devices are becoming harder to find as organizations drop out of this small niche business. Fortunately, the commercial trend toward higher density processes benefits total-dose hardness because oxides are thinner and surface inversion threshold are higher. By using hardening-by-design techniques and modern processes, readouts with adequate total-dose tolerance can be fabricated in commercial foundries for many space applications.

Displacement-damage-induced degradation was an important mechanism for early discrete infrared detectors. However, displacement damage was not a primary problem in the initially developed infrared detector arrays because the total-dose vulnerability of the detector arrays was the limiting mechanism, particularly for HgCdTe technology. As the total-dose-vulnerability problem in detector arrays has been solved, displacement-damage has again become a more important degradation mechanism. With material quality improvements (e.g., by lowering native defect concentrations), the devices become more susceptible to displacement-damage-induced defects. The displacement-damage thresholds of many detector materials is still high enough that displacement damage should not be a major issue except for the most demanding applications. One exception may be IR astronomy applications where even small increases in dark current can be problematic. Another exception is silicon-based detectors, which have the advantage of low-defect material developed by the commercial silicon industry. But this advantage makes silicon detectors susceptible to displacement-damage effects.

The transients and noise produced in infrared detectors by individual gamma photons and space radiation particles such as electrons, protons, and heavy ions remain an issue that is effectively as important now as it was when the technology was first developed and the problem recognized. Because the amplitude of the ionization-induced pulses in most detectors depends primarily on the detector thickness (where the thickness is the smallest dimension), use of thin detectors does result in smaller ionization-induced pulses. However, even these smaller pulses are usually larger than any optical signal and thus still interfere with device performance. The number of ionization-induced pulses depends on the average projected area of the detector and is controlled primarily by the optical area. The average projected area does not decrease much as the detector is thinned, and use of thinned detectors does not produce significantly improved tolerance against ionization-induced pulses and noise.

There have been some reasonably successful attempts to put microlenses on the detectors in order to shrink the electrical area of detectors while retaining the optical area. One major driver for this is to decrease the volume from which photo-diode leakage current is produced while retaining the full optical response, thus improving detector performance even without exposure to ionizing radiation. In addition, since ionizing particles would not be focused by these microlenses, the number of ionization-induced pulses would be decreased by this approach. Thus, microlenses should be a successful means to harden infrared detectors against fluxes of ionizing particles.

Many applications handle ionization-induced pulses and noise by recognizing and eliminating the unwanted pulses. If the array is oversampled either temporally or spatially, the ionization-induced pulses, which are temporally and spatially confined, can be eliminated without significantly degrading the optical signal. The recognition and elimination of ionization-induced pulses is usually done electronically off the focal plane and is quite effective if the application can stand the amount of oversampling necessary. This is the approach being taken to mitigate the cosmic ray induced transients in the James Webb Space Telescope (JWST). Design of effective cosmic ray rejection algorithms requires *a priori* knowledge of the effect of primary and secondary particles and detailed modeling of particle-induced charge collection and spreading in detector arrays [121].

B. CCDs

The study of CCD radiation effects remains as important as ever, particularly for space applications. Although active pixel sensors will take over for some cases, CCDs are still likely to have widespread use because they can often offer lower noise, stability of response, freedom from lag effects, and proven reliability.

Missions like the NASA's JWST and ESA's GAIA will have large CCD focal planes and there will be a need for better understanding of CTE traps. Even today, we cannot be sure of the defect inventory and how it changes with proton energy and silicon material. More work on CTE modeling and use of pre-injection techniques (to keep traps filled) is also needed.

RTS effects will be important for some space astronomy and Earth observation missions. Future work is likely to focus on just how many pixels are affected and the impact on radiometry and calibration strategies. The defect responsible is not yet identified.

Effects of low temperature proton irradiation and annealing for dark current spikes and CTE have not yet been studied in detail. Also, modeling of transients (including secondaries) will be important for missions such as JWST [121].

C. Active Pixel Sensors

APS technology shows promise for use in spaceborne applications that do not require the ultra-low noise performance achievable only with CCDs. Substantial leverage is to be expected for APS technology based on the strong consumer electronics demand. Both CCDs and APS devices can be hardened to total-ionizing-dose effects but displacement damage remains a concern. APS technology has the advantage of requiring only one charge transfer for signal readout, so they are not subject to proton-induced CCD charge transfer efficiency losses. However, other displacement damage issues such as dark current increases, dark spikes, and RTS behavior remain a concern with APS technology. In addition, transient effects and latch-up must always be considered in a space environment.

ACKNOWLEDGMENT

The authors would like to thank many of their colleagues for helpful discussions concerning available reference material. The second author would like to especially thank R. E. Mills of Raytheon Infrared Operations, in particular, for providing copies of two SPIE papers, on which he was a coauthor, and electronic versions of two figures from one of these papers.

REFERENCES

[1] A. G. Foyt, T. C. Harman, and J. P. Donnelly, "Type conversion and n-p junction formation in HgCdTe produced by proton bombardment," *Appl. Phys. Lett.*, vol. 18, p. 321, 1971.

[2] J. Melngailis, J. L. Ryan, and T. C. Harman, "Electron radiation damage and annealing of $Hg_{1-x}Cd_xTe$ at low temperature," *J. Appl. Phys.*, vol. 44, p. 2647, 1973.

[3] C. E. Mallon, J. A. Naber, J. F. Colwell, and B. A. Green, "Effects of electron irradiation on the electrical and optical properties of HgCdTe," *IEEE Trans. Nucl. Sci.*, vol. 20, p. 214, 1973.

[4] J. A. Naber, R. E. Leadon, H. T. Harper, B. A. Green, and C. E. Mallon, "Effects of electron irradiation at 80 K on ternary compounds containing Tellurium," in *Lattice Defects in Semiconductors*. London, U.K.: Inst. Physics, 1974, p. 321.

[5] F. D. Shepherd, Jr., "Radiation effects on the spectral response of HgCdTe," *IEEE Trans. Nucl. Sci.*, vol. 21, p. 34, 1974.

[6] R. E. Leadon and C. E. Mallon, "Model for defects in HgCdTe due to electron irradiation," *Infrared Phys.*, vol. 15, p. 259, 1975.

[7] C. E. Mallon, B. A. Green, R. E. Leadon, and J. A. Naber, "Radiation effects in $Hg_{1-x}Cd_xTe$," *IEEE Trans. Nucl. Sci.*, vol. 22, p. 2283, 1975.

[8] B. A. Green, R. E. Leadon, and C. E. Mallon, "Mobility changes produced by electron irradiation of n-type $Hg_{1-x}Cd_xTe$," *J. Appl. Phys.*, vol. 47, p. 3127, 1976.

[9] R. E. Leadon, C. E. Mallon, and J. A. Naber, "Effects of radiation on the low-temperature carrier recombination lifetimes in HgCdTe," in *Proc. Int. Conf. Radiation Effects in Semiconductors*. London, U.K.: Inst. Phys., 1977, p. 514.

[10] V. N. Brudnyi *et al.*, "Electrical and recombination characteristics of $Cd_xHg_{1-x}Te$ with electrons at $T = 300$ K," *Sov. Phys.—Semiconduct.*, vol. 11, p. 905, 1977.

[11] A. V. Voitsehovski, V. N. Brudnyi, Yu. V. Lilenko, M. A. Krivov, and A. S. Petrov, "High temperature defects in electron-irradiated semiconductors HgCdTe, PbSnTe," *Solid State Comm.*, vol. 31, p. 105, 1979.

[12] A. V. Voitsekhovskii, A. P. Kokhanenko, Yu. V. Lilenko, and A. S. Petrov, "Carrier lifetime in electron-irradiated p-Type HgCdTe crystals," *Sov. Phys.—Semiconduct.*, vol. 15, p. 386, 1981.

[13] ——, "Changes in the carrier lifetime in HgCdTe as a result of electron irradiation and subsequent annealing," *Sov. Phys.—Semiconduct.*, vol. 15, p. 930, 1981.

[14] A. V. Voitsekhovskii, Yu. V. Lilenko, A. P. Kokhanenko, and A. S. Petrov, "High temperature electron irradiation and isochronal annealing of p-Type HgCdTe crystals," *Rad. Eff.*, vol. 66, p. 79, 1982.

[15] A. V. Voitsekhovskii, A. P. Kokhanenko, S. F. Koverchik, Yu. V. Lilenko, and A. S. Petrov, "Characteristic features of the behavior of electron-irradiated $Hg_{1-x}Cd_xTe$ crystals subjected to various heat treatments," *Sov. Phys.—Semiconduct.*, vol. 17, p. 1119, 1983.

[16] A. V. Voitsekhovskii *et al.*, "Positron annihilation in electron-irradiated HgTe and $Hg_{1-x}Cd_xTe$ $(x = 0.2)$ crystals," *Sov. Phys.—Semiconduct.*, vol. 20, p. 514, 1986.

[17] A. V. Voitsekhovskii, A. P. Kokhanenko, A. S. Petrov, Yu. V. Lilenko, and A. D. Pogrebnyak, "Investigation of radiation defects in electron irradiated $Hg_{1-x}Cd_xTe$ crystals using positron annihilation," *Cryst. Res. Technol.*, vol. 23, p. 237, 1988.

[18] V. I. Ivanov-Omskii, N. V. Kutekhov, V. A. Smirnov, Sh. U. Yuldashev, and O. A. Gadaev, "Neutron irradiation of $Cd_xHg_{1-x}Te$," *Sov. Phys.—Semiconduct.*, vol. 26, p. 238, 1992.

[19] R. M. Broudy and V. J. Mazurczyk, "(HgCd)Te photoconductive detectors," in *Semiconductors and Semimetals*, R. K. Willardson and A. C. Beers, Eds. New York: Academic, 1981, vol. 18, pp. 157–111.

[20] M. B. Reine, A. K. Sood, and T. J. Tredwell, "Photovoltaic infrared detectors," in *Semiconductors and Semimetals*, R. K. Willardson and A. C. Beers, Eds. New York: Academic, 1981, vol. 18, pp. 201–311.

[21] A. H. Kalma and R. A. Cesena, "Radiation testing of trimetal infrared detectors," *IEEE Trans. Nucl. Sci.*, vol. 26, p. 4833, 1979.

[22] E. L. Divita, M. J. Holtzman, R. E. Mills, and D. T. Walsh, "Methodology for testing IR detectors in simulated nuclear radiation environments," *Proc. SPIE*, vol. 274, p. 1108, 1989.

[23] E. L. Divita, R. E. Mills, T. L. Koch, M. J. Gordon, R. A. Wilcox, and R. E. Williams, "Methodology for testing infrared focal plane arrays in simulated nuclear radiation environments," *Proc. SPIE*, vol. 50, p. 1686, 1992.

[24] N. D. Wilsey, C. S. Guenzer, B. Molnar, and W. J. Moore, "A comparison of fast neutron irradiation effects in photoconductive and photovoltaic InSb infrared detectors," *IEEE Trans. Nucl. Sci.*, vol. 22, p. 2448, 1975.

[25] H. T. Harper, B. A. Green, R. E. Leadon, and J. A. Naber, "Effects of irradiation on the electrical and optical properties of PbSnTe," *IEEE Trans. Nucl. Sci.*, vol. 21, p. 30, 1974.

[26] V. N. Brudnyi, A. V. Voitsekhovskii, M. A. Krivov, Yu. V. Lilenko, A. S. Petrov, and A. I. Potapov, "Electrical and recombination properties of electron-irradiated PbSnTe and PbSnSe crystals," *Sov. Phys.—Semiconduct.*, vol. 12, p. 885, 1987.

[27] R. R. Billups and W. L. Gardner, "Radiation damage experiments on PbS infrared detectors," *Infrared Phys.*, vol. 1, p. 199, 1961.

[28] B. Molnar, "Fast neutron irradiation damage on room temperature PbS detectors," *IEEE Trans. Nucl. Sci.*, vol. 21, p. 103, 1974.

[29] S. B. Atakulov, F. A. Zaitov, Yu. V. Matershev, K. E. Onarkulov, and A. E. Shavrov, "Diffusive nature of radiation-induced degradation of photoconducting lead sulfide films," *Sov. Phys.—Semiconduct.*, vol. 19, p. 1288, 1985.

[30] R. P. Day, R. A. Wallner, and E. A. Lodi, "An experimental study of energetic proton radiation effects on IRI lead sulfide infrared detectors," *Infrared Phys.*, vol. 1, p. 212, 1961.

[31] A. H. Kalma and C. J. Fischer, "Neutron damage mechanisms in silicon at 10 K," *IEEE Trans. Nucl. Sci.*, vol. 24, p. 2158, 1977.

[32] F. A. Junga, W. W. Anderson, and R. B. Emmons, "Effects of gamma irradiation on surface properties and detector properties of HgCdTe photoconductors," *IEEE Trans. Nucl. Sci.*, vol. 25, p. 1274, 1978.

[33] A. H. Kalma and M. A. Hopkins, "Ionizing radiation effects in HgCdTe MIS capacitors," *IEEE Trans. Nucl. Sci.*, vol. 28, p. 4083, 1981.

[34] J. R. Waterman and J. M. Killiany, "2 MeV electron irradiation effects in (Hg,Cd)Te CCDs," *IEEE Trans. Nucl. Sci.*, vol. 30, p. 4209, 1983.

[35] J. R. Waterman, "Radiation induced interface trap limited storage times in 10 micron cutoff wavelength (Hg.Cd)Te MIS capacitors," *IEEE Trans. Nucl. Sci.*, vol. 35, p. 1313, 1988.

[36] A. H. Kalma, "Nuclear and space radiation effects in infrared detectors," *Proc. SPIE*, vol. 217, p. 186, 1980.

[37] D. W. Domkowski, D. G. Feller, L. R. Johnson, C. I. Westmark, C. B. Norris, C. T. Fuller, and J. Bajaj, "Effects of 6 MeV electron irradiation on the electrical characteristics of LPE $Hg_{0.7}Cd_{0.3}Te$ mesa photodiodes," *IEEE Trans. Nucl. Sci.*, vol. 33, p. 1471, 1986.

[38] G. M. Williams, A. H. B. Vanderwyck, E. R. Blazejewski, R. P. Ginn, C. C. Li, and S. J. Nelson, "Gamma radiation response of MWIR and LWIR HgCdTe photodiodes," *IEEE Trans. Nucl. Sci.*, vol. 34, p. 1592, 1987.

[39] J. Favre, M. Konczykowski, and C. Blanchard, "Irradiation defects in $Hg_{1-x}Cd_xTe$ alloys," *Ann. Phys.*, p. 193, 14 colloq., 1989.

[40] G. Sarusi, D. Eger, A. Zemel, N. Mainzer, R. Goshen, and E. Weiss, "Degradation mechanisms of gamma irradiated LWIR HgCdTe photovoltaic detectors," *IEEE Trans. Nucl. Sci.*, vol. 37, p. 2042, 1990.

[41] J. E. Hubbs, G. A. Dole, M. E. Gramer, and D. C. Arrington, "Radiation effects characterization of infrared focal plane arrays using the Mosaic array test system," *Opt. Eng.*, vol. 30, p. 1739, 1991.

[42] J. R. Waterman and R. A. Schiebel, "Ionizing radiation effects in n-channel (Hg,Cd)Te MISFET's with anodic sulfide passivation," *IEEE Trans. Nucl. Sci.*, vol. 34, p. 1597, 1987.

[43] M. M. Moriwaki, J. R. Srour, L. F. Lou, and J. R. Waterman, "Ionizing radiation effects on HgCdTe MIS devices," *IEEE Trans. Nucl. Sci.*, vol. 37, p. 2034, 1990.

[44] M. M. Moriwaki, J. R. Srour, and R. L. Strong, "Charge transport and trapping in HgCdTe MIS devices," *IEEE Trans. Nucl. Sci.*, vol. 39, p. 2265, 1992.

[45] A. H. Kalma, R. A. Hartmann, and B. K. Janousek, "Ionizing radiation effects in HgCdTe MIS capacitors containing a photochemically-deposited SiO_2 layer," *IEEE Trans. Nucl. Sci.*, vol. 30, p. 4146, 1983.

[46] S. C. Chen and J. R. Srour, "Ionizing radiation effects on indium antimonide MIS devices," *IEEE Trans. Nucl. Sci.*, vol. 26, p. 4824, 1979.

[47] E. Finkman and S. E. Schacham, "Interface properties of various passivations of HgCdTe," *Proc. SPIE*, vol. 198, p. 1106, 1989.

[48] R. E. Mills, "Novel methods for cryogenic testing of infrared focal plane arrays in a Co60 radiation environment," *Proc. SPIE*, vol. 65, p. 1686, 1992.

[49] E. R. Blazejewski, G. M. Williams, A. H. Vanderwyck, D. D. Edwall, E. R. Gertner, J. Ellsworth, L. Fishman, S. R. Hampton, and H. R. Vydynath, "Advanced LWIR HgCdTe detectors for strategic applications," *Proc. SPIE*, vol. 278, p. 2217, 1994.

[50] D. T. Wilhelm, R. K. Purvis, A. Singh, D. Z. Richardson, R. A. Hahn, J. R. Duffey, and J. A. Ruffner, "Status of focal plane arrays (FPA's) for space-based applications," *Proc. SPIE*, vol. 307, p. 2217, 1994.

[51] X. Hu, X. Li, H. Lu, J. Zhao, H. Gong, and J. Fang, "Effect of gamma irradiation on room-temperature SWIR HgCdTe photodiodes," *Proc. SPIE*, vol. 85, p. 3553, 1998.

[52] X. Hu, K. X. Li, and J. Fang, "Influence of gamma irradiation on the performance of HgCdTe photovoltaic devices," *Proc. SPIE*, vol. 920, p. 3698, 1999.

[53] I. Arimura, J. N. Polky, and W. E. Maher, "Radiation effects analysis of a coherent laser detection system," *IEEE Trans. Nucl. Sci.*, vol. 24, p. 2315, 1977.

[54] G. M. Williams, A. H. B. Vanderwyck, E. R. Blazejewski, R. P. Ginn, C. C. Li, and S. J. Nelson, "Gamma radiation response of MWIR and LWIR HgCdTe photodiodes," *IEEE Trans. Nucl. Sci.*, vol. 34, p. 1592, 1987.

[55] J. E. Hubbs, G. A. Dole, M. E. Gramer, and D. C. Arrington, "Radiation effects characterization of infrared focal plane arrays using the mosaic array test system," *Opt. Eng.*, vol. 30, p. 1739, 1991.

[56] J. C. Pickel and M. D. Petroff, "Nuclear radiation induced noise in infrared detectors," *IEEE Trans. Nucl. Sci.*, vol. 22, p. 2456, 1975.

[57] E. A. Burke, J. J. Boyle, and H. J. Hummler, "Gamma-induced noise in CCDs," *IEEE Trans. Nucl. Sci.*, vol. 28, p. 4068, 1981.

[58] M. D. Petroff, J. C. Pickel, and M. P. Curry, "Low-level radiation effects in extrinsic infrared detectors," *IEEE Trans. Nucl. Sci.*, vol. 26, p. 4840, 1979.

[59] J. T. Montroy, R. Baron, G. C. Albright, J. Boisvert, and L. D. Flesner, " Energetic electron-induced impurity ionization in Si:As IBC detectors," *IEEE Trans. Nucl. Sci.*, p. 1307, 1988.

[60] R. E. Clement, J. C. Boisvert, and P. J. Sullivan, "Characterization and modeling of neutron induced transient response changes in Si : As IBC detectors," *IEEE Trans. Nucl. Sci.*, vol. 38, p. 1377, 1991.

[61] J. R. Janesick, *Scientific Charge-Coupled Devices*. Bellingham: SPIE, 2001.

[62] J. P. Theuwissen, *Solid-State Imaging With Charge-Coupled Devices*. Dordrecht, Germany: Kluwer, 1995.

[63] C. J. Marshall and P. W. Marshall, "Proton effects and test issues for satellite designers—Part B: Displacement damage effects," in *1999 IEEE NSREC Short Course Notes*, pp. IV-50–IV-110.
[64] G. R. Hopkinson, C. J. Dale, and P. W. Marshall, "Proton effects in CCDs," *IEEE Trans. Nucl. Sci.*, vol. 43, pp. 614–627, Apr. 1996.
[65] W. Boyle and G. Smith, "Charge coupled devices," *Bell Syst. Tech. J.*, vol. 49, pp. 587–593, 1970.
[66] J. M. Killiany, "Radiation effects on silicon charge-coupled devices," *IEEE Trans. Components, Hybrids Manuf. Tech.*, pp. 353–365, Dec. 1978.
[67] Mohsen and M. F. Tompsett, "The effects of bulk traps on the performance of bulk channel charge-coupled devices," *IEEE Trans. Electron. Devices*, vol. ED-21, pp. 701–712, Dec. 1974.
[68] N. S. Saks, "Investigation of bulk electron traps created by fast neutron irradiation in a buried n-channel CCD," *IEEE Trans. Nucl. Sci.*, vol. 24, pp. 2153–2157, Dec. 1977.
[69] T. Hardy, R. Murowinsky, and M. J. Deen, "Charge transfer efficiency in proton damaged CCD's," *IEEE Trans. Nucl. Sci.*, vol. 45, pp. 154–163, Apr. 1998.
[70] G. Prigozhin *et al.*, "Characterization of the radiation damage in the Chandra X-ray CCDs," *Proc. SPIE*, vol. 4140, pp. 123–134, Aug. 2000.
[71] G. R. Hopkinson, "Proton-induced charge transfer degradation at low operating temperatures," *IEEE Trans. Nucl. Sci.*, vol. 48, pp. 1790–1795, Dec. 2001.
[72] J. R. Srour, S. C. Chen, S. Othmer, and R. A. Hartman, "Radiation damage coefficients for silicon depletion regions," *IEEE Trans. Nucl. Sci.*, vol. 26, pp. 4784–4791, Dec. 1979.
[73] J. R. Srour and D. H. Lo, "Universal damage factor for radiation-induced dark current in silicon devices," *IEEE Trans. Nucl. Sci.*, vol. 47, pp. 2451–2459, Dec. 2000.
[74] N. S. Saks, "Interface state trapping and dark current generation in buried-channel charge-coupled devices," *J. App. Phys.*, vol. 53, no. 3, pp. 1745–1753, 1982.
[75] ——, "A technique for suppressing dark current generated by interface states in buried channel CCD imagers," *IEEE Electron. Device Lett.*, vol. 1, no. 7, July 1980.
[76] C. P. Cheng, "Radiation effects in n-buried channel CCD's fabricated with a hardened process," *IEEE Trans. Nucl. Sci.*, vol. 24, pp. 2190–2193, Dec. 1977.
[77] N. S. Saks, J. M. Killiany, P. R. Reid, and W. D. Baker, "A radiation hard MNOS CCD for low temperature applications," *IEEE Trans. Nucl. Sci.*, vol. 26, pp. 5074–5080, Dec. 1979.
[78] E. A. Burke, J. J. Boyle, and H. J. Huemmler, "Gamma-induced noise in CCDs," *IEEE Trans. Nucl. Sci.*, vol. 28, pp. 4068–4073, Dec. 1981.
[79] W. C. Jenkins, J. M. Killiany, and N. S. Saks, "Gamma radiation induced noise in a CCD imager," *IEEE Trans. Nucl. Sci.*, vol. 28, pp. 4161–4165, Dec. 1981.
[80] C. C. Liebe, "Charged particle-induced noise in camera systems," *IEEE Trans. Nucl. Sci.*, vol. 48, pp. 1541–1549, Aug. 2001.
[81] J. T. Trauger, "Sensors for the Hubble Space Telescope wide field and planetary cameras (1 and 2)," in *Proc. Conf. CCD's in Astronomy*, Tucson, AZ, Sept. 6–8, 1989. Astronomical Soc. Pacific, p. 217-230, 1990. See also: B. E. Woodgate, "The use of CCD's in the Space Telescope Imaging Spectrograph (STIS)," ibid, pp. 237–257.
[82] K. P. Klaasen, M. Clarey, and J. Janesick, "Charge-coupled device television camera for NASA's Galileo Mission to Jupiter," *Opt. Eng.*, vol. 23, pp. 334–342, 1984.
[83] J. R. Srour, Z. Shanfield, R. A. Hartmann, S. Othmer, and D. M. Newberry, "Permanent damage introduced by single particles incident on silicon devices," *IEEE Trans. Nucl. Sci.*, vol. 30, pp. 4526–4532, Dec. 1983.
[84] J. R. Srour and R. A. Hartmann, "Effects of single neutron interactions in silicon integrated circuits," *IEEE Trans. Nucl. Sci.*, vol. 32, pp. 4195–4200, Dec. 1985.
[85] J. R. Srour, R. A. Hartmann, and K. S. Kitazaki, "Permanent damage introduced by single proton interactions in silicon devices," *IEEE Trans. Nucl. Sci.*, vol. 33, pp. 1597–1606, Dec. 1986.
[86] J. Janesick, T. Elliott, and F. Pool, "Radiation damage in scientific charge-coupled devices," *IEEE Trans. Nucl. Sci.*, vol. 36, pp. 572–578, Jun. 1988.
[87] P. W. Marshall, C. J. Dale, E. A. Burke, G. P. Summers, and G. E. Bender, "Displacement damage extremes in silicon depletion regions," *IEEE Trans. Nucl. Sci.*, vol. 36, pp. 1831–1839, Dec. 1989.
[88] J. R. Srour and R. A. Hartmann, "Enhanced displacement damage effectiveness in irradiated silicon devices," *IEEE Trans. Nucl. Sci.*, vol. 36, pp. 1825–1830, Dec. 1989.
[89] G. R. Hopkinson and Ch. Chlebek, "Proton damage effects in an EEV CCD imager," *IEEE Trans. Nucl. Sci.*, vol. 36, pp. 1865–1871, Dec. 1989.
[90] P. W. Marshall, C. J. Dale, and E. A. Burke, "Proton-induced displacement damage distributions in silicon microvolumes," *IEEE Trans. Nucl. Sci.*, vol. 37, pp. 1776–1783, Dec. 1990.
[91] M. S. Robbins, "High-energy proton-induced dark signal in silicon charge coupled devices," *IEEE Trans. Nucl. Sci.*, vol. 47, pp. 2473–2479, Dec. 2000.
[92] V. A. J. Van Lint, G. Gigas, and J. Barengoltz, "Correlation of displacement effects produced by electrons, protons and neutrons in silicon," *IEEE Trans. Nucl. Sci.*, vol. 22, pp. 2663–2668, Dec. 1975.
[93] C. J. Dale, L. Chen, P. J. McNulty, P. W. Marshall, and E. A. Burke, "A comparison of Monte Carlo and analytical treatments of displacement damage in Si microvolumes," *IEEE Trans. Nucl. Sci.*, vol. 41, pp. 1974–1983, Dec. 1994.
[94] Akkerman, J. Barak, M. B. Chadwick, J. Levinson, M. Murat, and Y. Lifshitz, "Updated NIEL calculations for estimating the damage induced by particles and γ rays in Si and GaAs," *Radiation Phys. Chemistry*, vol. 62, pp. 301–310, 2001.
[95] A. Holmes-Seidle, A. Holland, and S. Watts, "The impact of space protons in x-ray sensing with charge coupled devices (CCD's)," *IEEE Trans. Nucl. Sci.*, vol. 43, pp. 2998–3003, Dec. 1996.
[96] A. Yamashita, T. Dotani, M. Bautz, G. Crew, H. Ezuka, K. Gendreau, T. Kotani, K. Mitsuda, C. Otani, A. Rasmussen, G. Ricker, and H. Tsunemi, "Radiation damage to charge coupled devices in the space environment," *IEEE Trans. Nucl. Sci.*, vol. 44, pp. 847–853, June 1997.
[97] J. Holtzmam *et al.*, "The performance and calibration of WFPC2 on the Hubble Space Telescope," *Publ. Astron. Soc. Pac.*, vol. 107, pp. 156–178, 1995.
[98] Waczynski, E. J. Polidan, P. W. Marshall, R. A. Reed, S. D. Johnson, R. J. Hill, G. S. Delo, E. J. Wassell, and E. S. Cheng, "A comparison of charge transfer efficiency measurement techniques on proton damaged CCD's for the Hubble Space Telescope wide-field camera 3," *IEEE Trans. Nucl. Sci.*, vol. 48, pp. 1807–1814, Dec. 2001.
[99] R. A. Kimble, P. Goudfrooij, and R. L. Gilliland, "Radiation damage effects on the CCD detector of the space telescope imaging spectrograph," *Proc. SPIE*, vol. 4013, pp. 532–545, July 2000.
[100] G. R. Hopkinson, "Proton-induced changes in CTE for n-channel CCD's and the effect on star tracker performance," *IEEE Trans. Nucl. Sci.*, vol. 47, pp. 2460–2465, Dec. 2000.
[101] C. Dale, P. Marshall, B. Cummings, L. Shamey, and A. Holland, "Displacement damage effects in mixed particle environments for shielded spacecraft CCDs," *IEEE Trans. Nucl. Sci.*, vol. 40, pp. 1628–1637, Dec. 1993.
[102] D. Gallagher, R. Demara, G. Emerson, W. Frame, and A. Delamere, "Monte Carlo model for describing charge transfer in irradiated CCDs," *Proc. SPIE*, vol. 3301, pp. 80–88, 1998.
[103] R. H. Philbrick, "Modeling the impact of preflushing on CTE in proton irradiated CCD-based detectors," *IEEE Trans. Nucl. Sci.*, vol. 49, pp. 559–567, Apr. 2002.
[104] G. R. Hopkinson, "Proton damage effects on p-channel CCDs," *IEEE Trans. Nucl. Sci.*, vol. 46, pp. 1790–1796, Dec. 1999.
[105] J. Spratt, B. C. Passenheim, and R. E. Leadon, "The effects of nuclear radiation on P-channel CCD imagers," in *1997 IEEE Radiation Effects Data Workshop Rec.*, 1998, pp. 116–121.
[106] C. Bebek *et al.*, "Proton radiation damage in P-channel CCD's fabricated on high-resistivity silicon," *IEEE Trans. Nucl. Sci.*, vol. 49, pp. 1221–1225, June 2002.
[107] I. H. Hopkins and G. R. Hopkinson, "Further measurements of random telegraph signals in proton irradiated CCDs," *IEEE Trans. Nucl. Sci.*, vol. 42, pp. 2074–2081, Dec. 1995.
[108] T. L. Miller, D. A. Thompson, M. B. Elzinga, T. -H. Lee, B. C. Passenheim, and R. E. Leadon, "Experimental evaluation of high speed CCD imager radiation effects using Co60 and proton radiation," in *1993 IEEE Radiation Effects Data Workshop Rec.*, 1994, pp. 56–63.
[109] K. P. Klaasen *et al.*, "Inflight performance characteristics, calibration, and utilization of the Galileo SSI camera," *Opt. Eng.*, vol. 36, pp. 3001–3027, 1997.
[110] M. S. Robbins, T. Roy, S. J. Hedges, A. Holmes-Siedle, A. K. McKemey, and S. J. Watts, "Quality control and monitoring of radiation damage in charge coupled devices at the Stanford Linear Collider," *IEEE Trans. Nucl. Sci.*, vol. 40, pp. 1561–1566, Dec. 1993.
[111] B. Burke and S. A. Gajar, "Dynamic suppression of interface.-state dark current in buried channel CCDs," *IEEE Trans. Electron. Devices*, vol. 38, pp. 285–290, Feb. 1991.

[112] E. R. Fossum, "CMOS image sensors: Electronic camera-on-a-chip," *IEEE Trans. Electron. Devices*, vol. 44, pp. 1680–1698, Oct. 1997.
[113] M. Cohen and J. P. David, "Radiation effects on active pixel sensors," in *RADECS Proc.*, 1999, pp. 450–456.
[114] ——, "Radiation-induced dark current in CMOS active pixel sensors," *IEEE Trans. Nucl. Sci.*, vol. 47, pp. 2485–2491, Dec. 2000.
[115] J. Bogaerts and B. Dierickx, "Total dose effects on CMOS active pixel sensor," in *Proc. SPIE Photonics West*, vol. 4134, San Jose, CA, Jan. 24, 2000.
[116] G. R. Hopkinson, "Radiation effects in a CMOS active pixel sensor," *IEEE Trans. Nucl. Sci.*, vol. 47, pp. 2480–2484, Dec. 2000.
[117] J. Bogaerts, B. Dierickx, and R. Mertens, "Enhanced dark current generation in proton-irradiated CMOS active pixel sensors," *IEEE Trans. Nucl. Sci.*, vol. 49, pp. 1513–1521, June 2002.
[118] ——, "Random telegraph signals in a radiation-hardened CMOS active pixel sensor," *IEEE Trans. Nucl. Sci.*, vol. 49, pp. 249–257, Feb. 2002.
[119] E.-S. Eid, T. Y. Chan, E. R. Fossum, R. H. Tsai, R. Spagnuolo, J. Deily, W. B. Byers, Jr., and J. C. Peden, "Design and characterization of ionizing radiation-tolerant CMOS APS image sensors up to 30 Mrd(Si) total dose," *IEEE Trans. Nucl. Sci.*, vol. 48, pp. 1796–1806, Dec. 2001.
[120] C. J. Marshall, K. A. LaBel, R. A. Reed, P. W. Marshall, W. B. Myers, C. Conger, J. Peden, E.-S. Eid, M. R. Jones, S. Kniffen, G. Gee, and J. Pickel, "Heavy ion transient characterization of a hardened-by-design active pixel sensor array," in *2002 IEEE Radiation Effects Data Workshop*, July 2002, pp. 187–193.
[121] J. C. Pickel, R. A. Reed, R. Ladbury, B. Rauscher, P. W. Marshall, T. M. Jordan, B. Fodness, and G. Gee, "Radiation-induced collection charge in infrared detector arrays," *IEEE Trans. Nucl. Sci.*, vol. 49, pp. 2822–2829, Dec. 2002.
[122] X. Belredon, J.-P. Davis, D. Lewis, T. Beauchene, V. Pouget, S. Barde, and P. Magnan, "Heavy ion-induced charge collection mechanisms in CMOS active pixel sensor," *IEEE Trans. Nucl. Sci.*, vol. 49, pp. 2836–2843, Dec. 2002.